COMPLEX HAMILTONIAN DYNAMICS

Tassos BOUNTIS

Department of Mathematics and Center for Research and Applications of Nonlinear Systems (CRANS), University of Patras, GR–26500, Rion, Patras, Greece

Lecture 3:

Complex Statistics at the Edge of Chaos:
Applications to Statistical Mechanics and Galactic Dynamics

2nd PhD School on "Mathematical Modeling of Complex Systems",

Pescara, Italy, July 16 - 28, 2012

Ph.D. School on "Mathematical Modeling of Complex Systems", Patras, Greece 18 - 29 July, 2011

http://www.math.upatras.gr/ phdsch11

1. Mathematical Foundations of Complexity

Robert MacKay (Warwick, UK), Jeff Johnson (Open University UK), Steven Bishop (London, UK)

2. Physics of Complex Systems

Nico Gray, Tom Mullin (Manchester, UK), Tassos Bountis, Ko van der Weele (Patras, GR), Pierre Gaspard, Thomas Gilbert, D. Andrieux (Brussels, B), Devaraj van der Meer (Twente, NL)

3. Complexity in Biology and Neuronal Dynamics

Erik Mosekilde (Lyngby, DK), Juergen Kurths (Berlin, D), Anastasios Bezerianos (Patras, GR)

4. Complex Systems in Economics and Sociology

Rosario Mantegna (Palermo, I), Dirk Helbing (Zurich, CH)

Complex Hamiltonian Dynamics

Tassos Bountis and Haris Skokos

Springer Complexity series 2011

Chapter 1. Fundamental concepts of Lyapunov and Poincaré

Chapter 2. Hamiltonian Systems of Few Degrees of Freedom

Chapter 3. Local and Global Stability of Motion

Chapter 4. Normal Modes, Symmetries and Stability

Chapter 5. Efficient Indicators of Stable and Chaotic Motion

Chapter 6. FPU Recurrences and the Transition from Weak to Strong Chaos

Chapter 7. Localization and Diffusion in Nonlinear 1-Dimensional Lattices

Chapter 8. Complex Statistics of Quasi-Stationary States

Contents

1. Sums of Random Variables and the Central Limit Theorem

2. Nonextensive Statistical Mechanics and q-Gaussians

3. Pdfs of Chaotic States in Area–Preserving Maps

4. Quasi–Stationary Chaotic States in Fermi Pasta Ulam Chains

5. Weakly and Strongly Chaotic Orbits in a Barred Galaxy Model

6. Conclusions

Sums of Random Variables and the Central Limit Theorem

The approach we shall follow is in the spirit of the Central Limit Theorem (CLT). In particular, we focus on chaotic regions of: (a) **area–preserving maps**

$$\begin{cases} x_{n+1} = f(x_n, y_n) \\ y_{n+1} = g(x_n, y_n) \end{cases} \tag{1}$$

and (b) N**–degree–of–freedom Hamiltonian systems**

$$\frac{dq_k}{dt} = \frac{\partial H}{\partial p_k}, \quad \frac{dp_k}{dt} = -\frac{\partial H}{\partial q_k}, \quad k = 1, 2, \ldots, N \tag{2}$$

and construct **distributions** of rescaled sums of M values of an observable $\eta_i = \eta(t_i)$, $i = 1, \ldots, M$, which is a linear combination of the variables (x_n, y_n), or $(q_n(t), p_n(t))$ of the problem. These are viewed as **independent random variables** in the **limit of large** $M(\to \infty)$ and we evaluate **their sums** for a **large number** N_{ic} of initial conditions:

$$S_M^{(j)} = \sum_{i=1}^{M} \eta_i^{(j)}, \quad j = 1, \ldots, N_{\text{ic}} \tag{3}$$

We then study the **probability density functions (pdfs)** of the variables $S_M^{(j)}$, centered about their **mean value** $\langle S_M^{(j)} \rangle$ and rescaled by their **standard deviation** σ_M

$$s_M^{(j)} \equiv \frac{1}{\sigma_M}\left(S_M^{(j)} - \langle S_M^{(j)} \rangle\right) = \frac{1}{\sigma_M}\left(\sum_{i=1}^{M} \eta_i^{(j)} - \frac{1}{N_{\text{ic}}} \sum_{j=1}^{N_{\text{ic}}} \sum_{i=1}^{M} \eta_i^{(j)}\right) \tag{4}$$

where

$$\sigma_M^2 = \frac{1}{N_{\text{ic}}} \sum_{j=1}^{N_{\text{ic}}} \left(S_M^{(j)} - \langle S_M^{(j)} \rangle\right)^2 = \langle S_M^{(j)2} \rangle - \langle S_M^{(j)} \rangle^2. \tag{5}$$

If our variables are **random**, or **belong to uniformly ergodic regimes of deterministic systems**, when we plot the normalized distribution of probabilities $P(s_M^{(j)})$ as a function of $s_M^{(j)}$, , we expect to find **in the spirit of the classical CLT**:

$$P(s_M^{(j)}) = a e^{-\beta s_M^{(j)2}} \tag{6}$$

i.e a **Gaussian pdf**.

However, in regimes of **"weak chaos"** of many **conservative systems**, these distributions are well–approximated by different pdfs, the most ubiquitous of them being the q**-Gaussian**:

$$P(s_M^{(j)}) = a e_q^{-\beta s_M^{(j)2}} \equiv a\left(1-(1-q)\beta s_M^{(j)2}\right)^{\frac{1}{1-q}} \qquad (7)$$

where q is the **Tsallis entropy index**, β is **a free parameter** and a **a normalization constant**. Expression (7) is a generalization of the Gaussian, since in the limit $q \to 1$ we have $lim_{q\to 1} e_q^{-\beta x^2} = e^{-\beta x^2}$. If $1 \leq q < 3$, (7) is normalized for an appropriate choice of $a(\beta)$.

As we shall demonstrate, there are **many interesting cases of conservative systems**, where chaotic orbits are strongly influenced by **"stickiness" phenomena** and produce **long–lived quasi–stationary states** (QSS), whose pdfs are well–approximated by q–Gaussians. These, however, **do not always converge to a q gaussian, but evolve, through a sequence of QSS**, which we seek to identify the limit $t \to \infty$.

Nonextensive Statistical Mechanics and q-Gaussians

Multi–particle systems belong to **different "universality" classes**, according to their thermostatistics. In the most widely studied **Boltzmann–Gibbs class**, if the system can be at any one of $i = 1, 2, ..., W$ states with probability p_i, its entropy is given by the famous formula

$$S_{BG} = -k \sum_{i=1}^{W} p_i ln p_i \tag{8}$$

where k is Boltzmann's constant, provided, of course,

$$\sum_{i=1}^{W} p_i = 1 \tag{9}$$

The BG entropy satisfies the property of **additivity**, i.e. if A and B are two statistically independent systems, the probability to be in their union is $p_{i,j}^{A+B} = p_i^A p_j^B$ and this necessitates that the entropy of the joint state obey

$$S_{BG}(A + B) = S_{BG}(A) + S_{BG}(B) \tag{10}$$

At thermal equilibrium, the p_i **that optimize the BG entropy**, subject to ((9)) and a given energy spectrum E_i and temperature T are:

$$p_i = \frac{e^{-\beta E_i}}{Z_{BG}}, \qquad Z_{BG} = \sum_{i=1}^{W} e^{-\beta E_i} \tag{11}$$

where $\beta = 1/kT$ and Z_{BG} is the so–called partition function. For a **continuum set of states depending on one variable**, x, the optimal probability density function (pdf) corresponding to BG statistics subject to ((9)), zero mean and given variance V is, of course, the well–known Gaussian $p(x) = e^{-x^2/2V}/\sqrt{2V}$.
Another important property of the BG entropy is that it is **extensive**,

$$lim_{N\to\infty} \frac{S_{BG}}{N} < \infty \tag{12}$$

i.e. it grows **linearly** as a function of the number of degrees of freedom N of the system. But then, what about **many physically important systems** that are **not extensive**?

There are **many examples of non–extensive systems**, like: **self–gravitating systems of finitely many mass points**, interacting black holes, ferromagnetic models, systems with **long range forces**, in which **strong correlations and power laws** are dominant.

In deterministic dynamics, for instance, **chaos does not always mean exponential instability**, as there are regimes of **"weak chaos"**, where "stickiness phenomena" occur **on or near the boundary** of regions of regular motion called **'edge of chaos'**, where **Lyapunov exponents are zero** and orbits separate linearly from each other.

It is for these type of situations that Tsallis proposed a different form of entropy [Tsallis,2009]

$$S_q = k\frac{1-\sum_{i=1}^{W} p_i^q}{q-1} \text{ with } \sum_{i=1}^{W} p_i = 1 \tag{13}$$

depending on an index q, where $i = 1, \ldots, W$ counts the microstates of the system occurring with probability p_i and k is the Boltzmann constant.

Just as the Gaussian distribution represents an **extremal of the BG entropy** ((8)), so is the **q–Gaussian pdf** obtained as a **maximum** (for $q > 0$) or a **minimum** (q<0) of the Tsallis entropy ((13)).

$$p(x) = ae_q^{-\beta x^2} \equiv a\left(1 - (1-q)\beta x^2\right)^{\frac{1}{1-q}} \tag{14}$$

for a continuum set of states.

The Tsallis entropy is **not additive**, as

$$S_q(A+B) = S_q(A) + S_q(B) + k(1-q)S_q(A)S_q(B) \tag{15}$$

and hence **is not extensive**. It thus offers the possibility of studying cases where the A, B subsystems mentioned above are strongly correlated.

Systems characterized by these properties are said to have **complex statistics**, which is significantly different from BG systems.

Nonextensive Thermodynamics

If we have a discrete set of states $j = 1, 2, ..., W$, we define the escort probabilities

$$P_i = \frac{p_i^q}{\sum_{j=1}^{W} p_j^q} \tag{16}$$

Given the constraints (9) and

$$< E_i >_q = \sum_{j=1}^{W} P_i E_i = U_q \tag{17}$$

we find that **the distribution that extremizes the Tsallis entropy** S_q is the q-Gaussian

$$p_i = \frac{e_q^{-\beta_q (E_i - U_q)}}{\tilde{Z}_q} \tag{18}$$

where the partition function $\tilde{Z}_q$ is given by

$$\tilde{Z}_q = \sum_{i=1}^{W} e_q^{-\beta_q (E_i - U_q)} \tag{19}$$

and β_q is the Lagrange multiplier associated with constraint (12)

$$\beta_q = \frac{\beta}{\sum_{j=1}^{W} p_j^q} \tag{20}$$

From the above one can prove that **the fundamental thermodynamical equations have the same form as the corresponding BG expressions with all variables indexed by** q, and $\beta = 1/kT$:

$$S_q = k ln_q \tilde{Z}_q, \quad \frac{1}{T} = \frac{\partial S_q}{\partial U_q}, \quad F_q = U_q - TS_q = -\frac{1}{T} ln_q Z_q \tag{21}$$

and $lnZ_q = ln\tilde{Z}_q - \beta U_q$.

Pdfs of Chaotic States in Area–Preserving maps

Consider the perturbed MacMillan map, which occurs in the study of equilibrium configurations of Ablowitz–Ladik Discrete Nonlinear Schrodinger Equations:

$$\begin{cases} x_{n+1} = y_n \\ y_{n+1} = -x_n + 2\mu \frac{y_n}{1+y_n^2} + \epsilon y_n \end{cases} \tag{22}$$

with parameters ϵ, μ. Since its Jacobian is 1, (22) is area-preserving.

We have analyzed the histogram of their normalized sums for a range of parameters (ϵ, μ) and have identified some generic classes of q-**Gaussians**, **exponentials**, $\sim e^{-k|z|}$ or **Gaussians**. Monitoring their time evolution for increasing number of iterations N, we observe the occurrence of different QSS, which we present with the corresponding phase space plots in the Figures below.

ϵ	0.2	0.5	0.9	1.2	1.6	1.8
L_{max}	0.0867	0.082	0.0875	0.0513	0.0495	0.05876

Table 1: Maximal Lyapunov exponents for $\mu = 0.6$ and $\epsilon = 0.2, 0.5, 0.9, 1.2, 1.6, 1.8$.

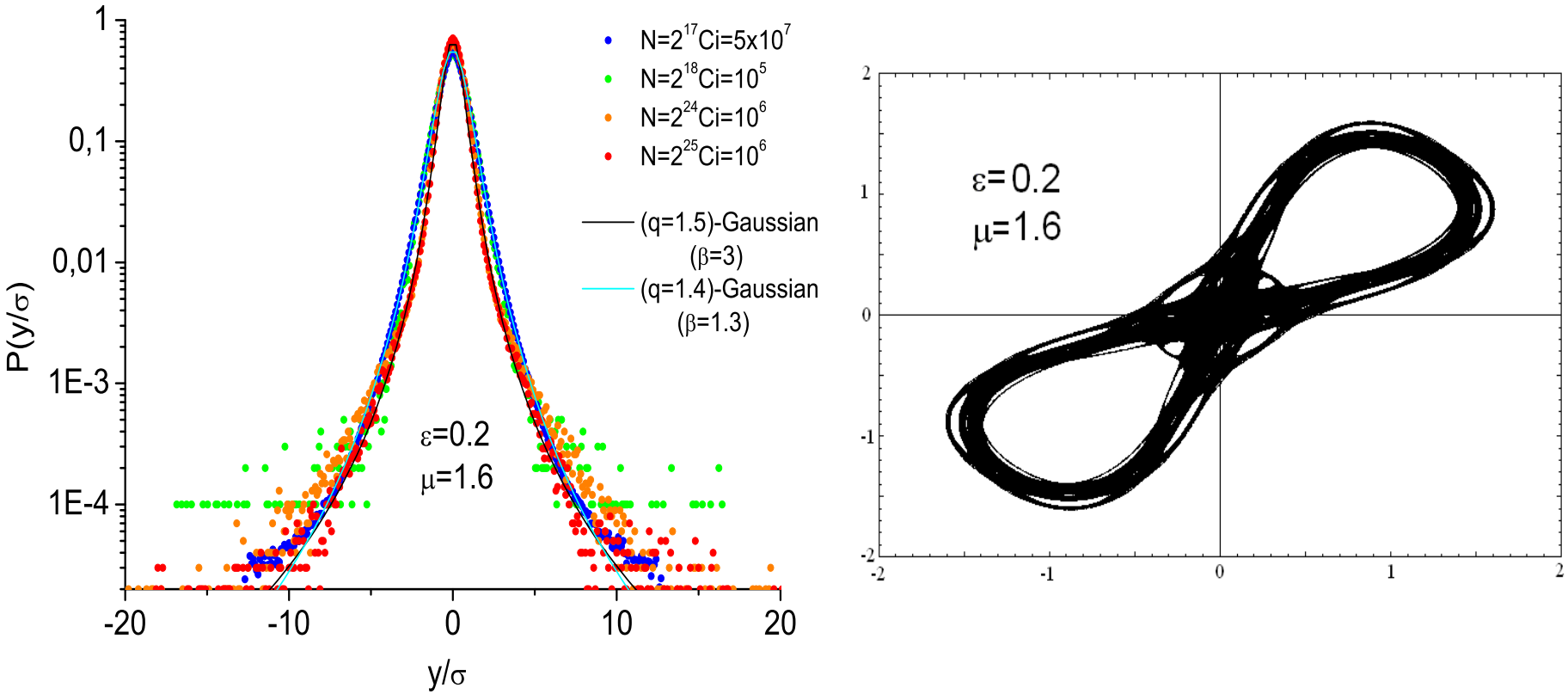

Figure 1. Tendency away from a Gaussian: Dynamical and statistical behavior of chaotic orbits of the MacMillan map for parameter values $\mu = 1.6$, and $\epsilon = 0.2$. Left: The pdfs of the normalized sums of iterates. Right: The corresponding phase space plot. N is the number of iterates and N_{ic} is the number of initial conditions randomly chosen from a square $(0, 10^{-6}) \times (0, 10^{-6})$.

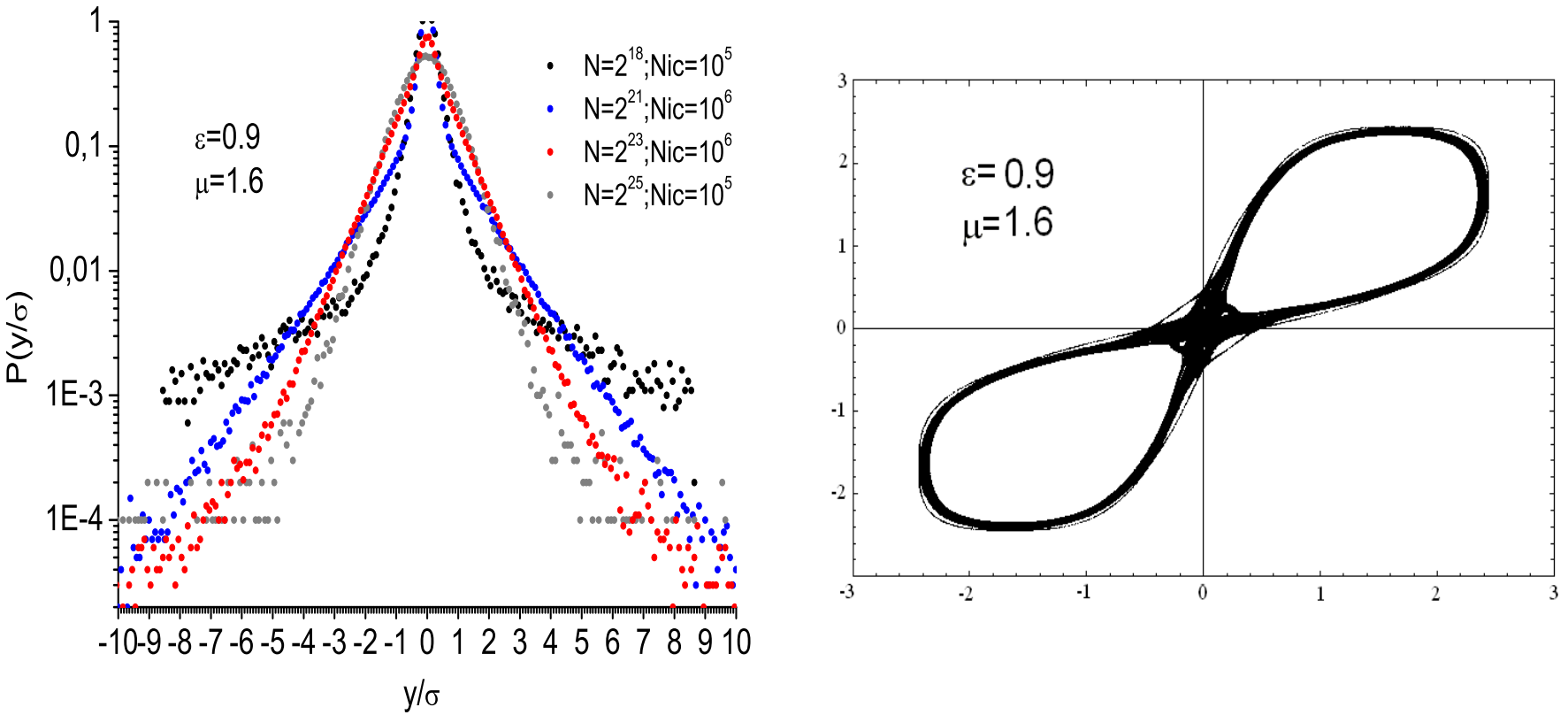

Figure 2. Tendency towards a Gaussian: Dynamical and statistical behavior of chaotic orbits of the MacMillan map for parameter values $\mu = 1.6$, and $\epsilon = 0.9$. Left: The pdfs of the normalized sums of iterates. Right: The corresponding phase space plot. N represents the number of (summed) iterates and N_{ic} is the number of initial conditions randomly chosen from a square $(0, 10^{-6}) \times (0, 10^{-6})$.

A. The $\epsilon = 0.9$, ($\mu = 1.6$) case: Towards a Gaussian

The $\epsilon = 0.9$ case is a typical example producing time–evolving pdfs. Figures 1 shows that the corresponding phase space plots yield a simple chaotic region in phase space around two islands, yet the corresponding pdfs do not converge to a single distribution, rather they pass from q-**Gaussians** to **triangular** to **Gaussian** distributions.

There exist at least **three long–lived QSS** whose iterates generate pdfs passing through different shapes. Consequently, for $i = 1 \ldots N = 2^{16}$, a QSS is produced whose pdf is a $(q = 1.6)$–Gaussian whose β increases with increasing N. This is most likely due to a **"stickiness"** effect around islands of regular motion.

Figures 3 and 4 below show phase space plots for a number of iterates N. Note that for $N = 1 \ldots 2^{16}$, a 'figure eight' chaotic region is formed around two islands. But for $N > 2^{16}$, a more complex structure emerges, as iterates stick around new islands, and **phase space statistics passes through a sequence of quasi-stationary states.**

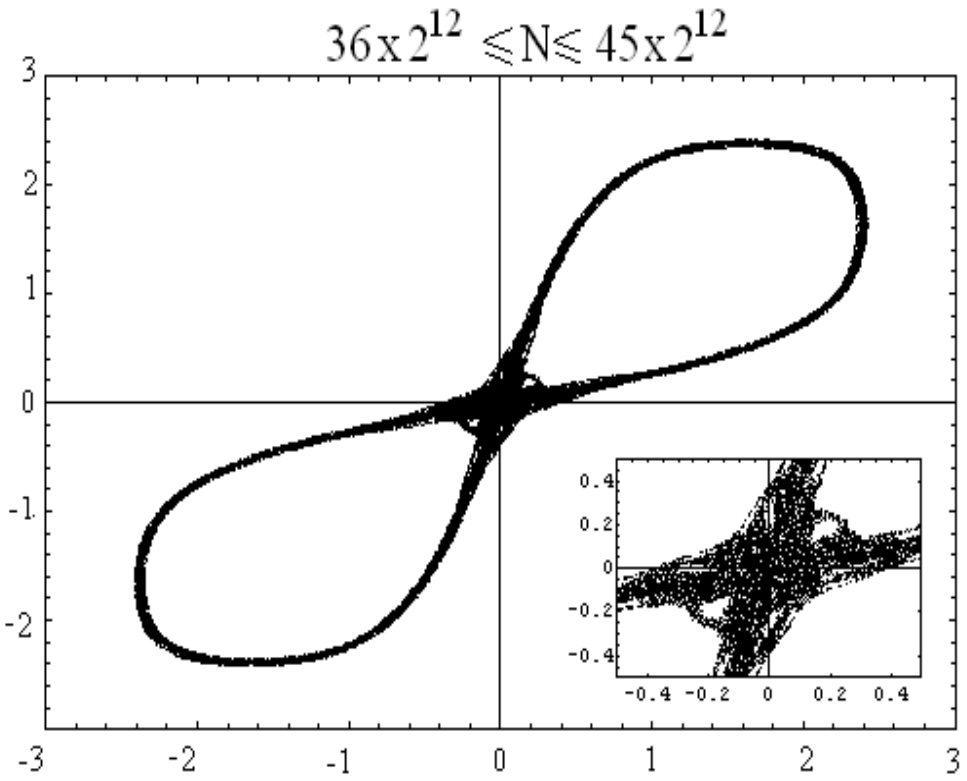

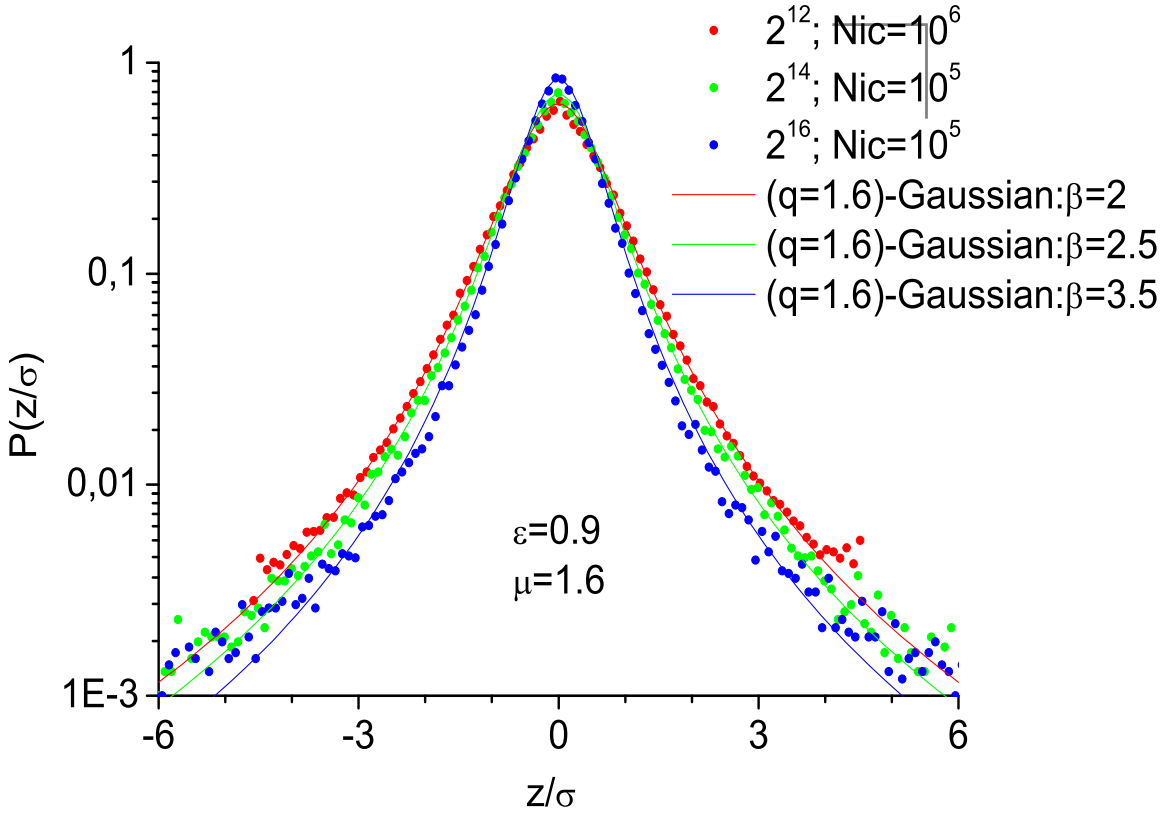

Figure 3. $\epsilon = 0.9$, $\mu = 1.6$ MacMillan map phase space plots (first panel) and the corresponding PDFs (second panel) of the re-normalized sums as the number of iterates $i = 1 \ldots N, N \leq 10^{16}$ increases, starting from a randomly chosen initial condition in a square $(0, 10^{-6}) \times (0, 10^{-6})$.

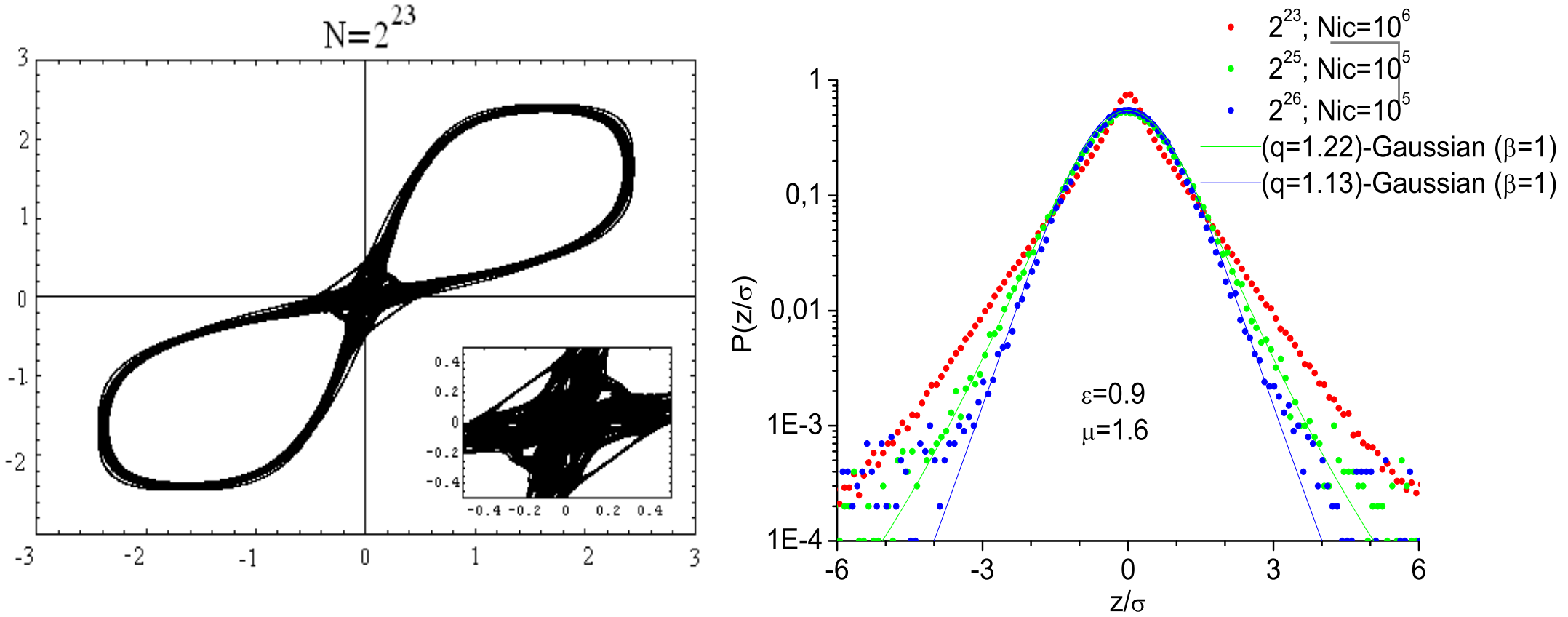

Figure 4. $\epsilon = 0.9$, $\mu = 1.6$ MacMillan map phase space for $i = 1 \ldots N, N \geq 2^{23}$ plot iterates, starting from a randomly chosen initial condition in a square $(0, 10^{-6}) \times (0, 10^{-6})$ and the corresponding pdfs (right panel).

Thus, more than one QSS coexist whose pdfs form a sequence of different $(q \neq 1)$–Gaussians. As we see in Figure 3 that this sequence of QSS for $N \leq 2^{21}$ produces a distribution where central part is still well–described by a $(q = 1.6)$**–Gaussian**.

However, as we continue to iterate the map to $N = 2^{23}$, this $(q = 1.6)$–Gaussian passes through a superposition of states characterized by **triangular distributions**. From here on, as $N > 2^{23}$, the central part of the pdfs become q–Gaussians with $q \to 1$ (see Figure 4) and a true **Gaussian** is expected in the limit ($N \to \infty$).

B. The $\epsilon = 1.2$, ($\mu = 1.6$) cases: Towards a q Gaussian

Let us now analyze the cases $\epsilon = 1.2$, whose maximum Lyapunov exponent is $L_{max} \approx 0.05$. In Figure 5 iterates show a **diffusive behavior** that spreads around islands of a higher order resonance, as iterations reach $N = 2^{19}$.

The central part of the pdfs **converges to a** $(q = 1.6)$**–Gaussian** for $N \leq 2^{16}$ (left panel of Fig. 5). Then, orbits diffuse outward and even the tail of the pdf converges to a $(q = 1.6)$-Gaussian (right panel of Fig. 5). For larger N, diffusion ceases at the q–Gaussian of Figure 6.

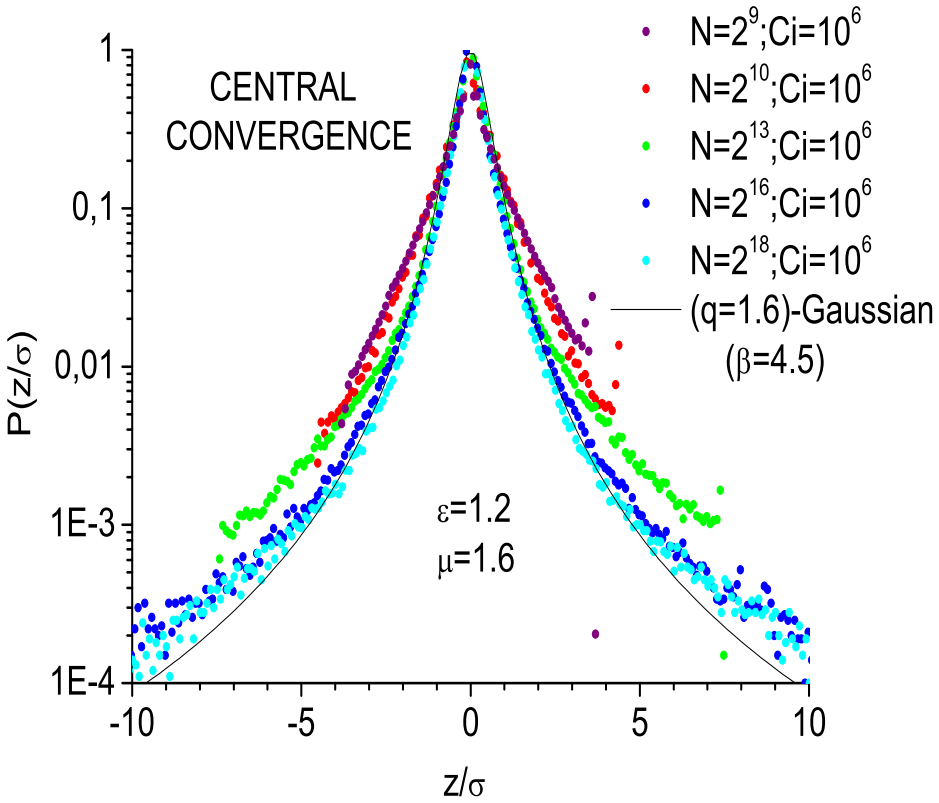

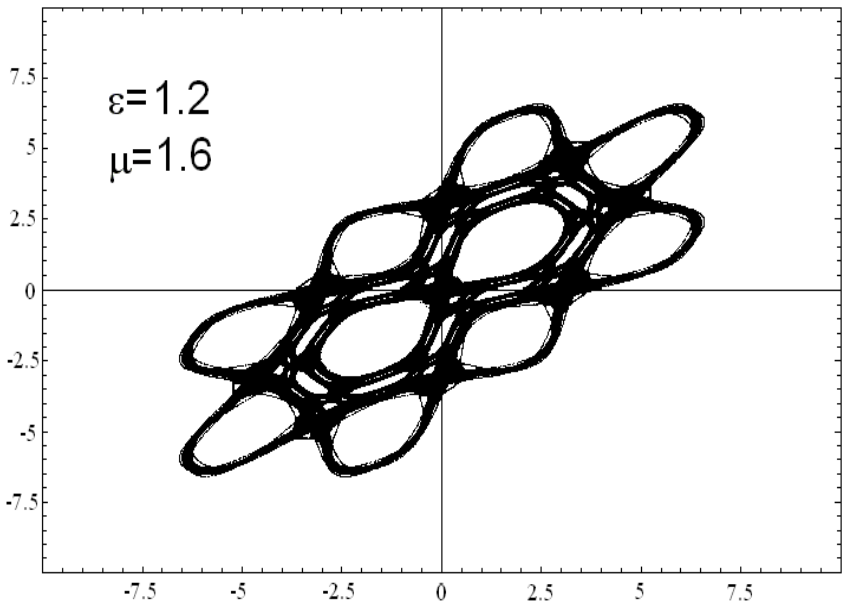

Figure 5. Dynamical and statistical behavior of chaotic orbits of the MacMillan map for $\mu = 1.6$, and $\epsilon = 1.2$. On the right the phase space plot and on the left the pdfs of the normalized sums of iterates.

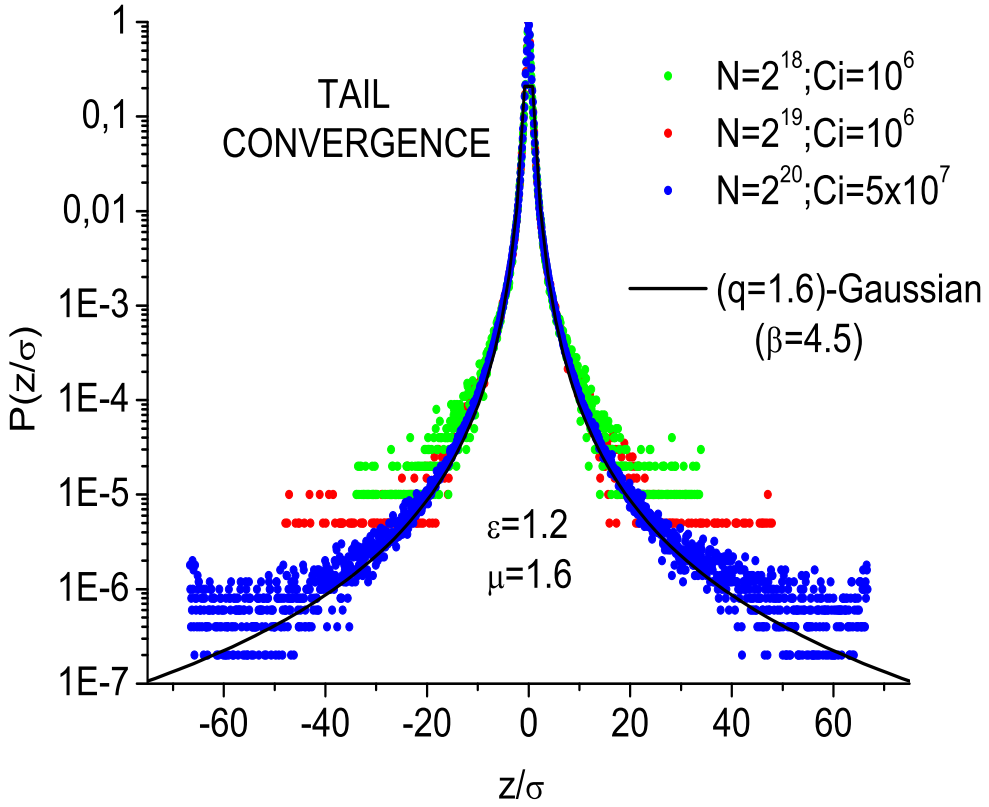

Figure 6. Tail convergence of the q–Gaussian for $\mu = 1.6$, and $\epsilon = 1.2$ depicting the pdfs for $N > 2^{18}$ numbers of iterates.

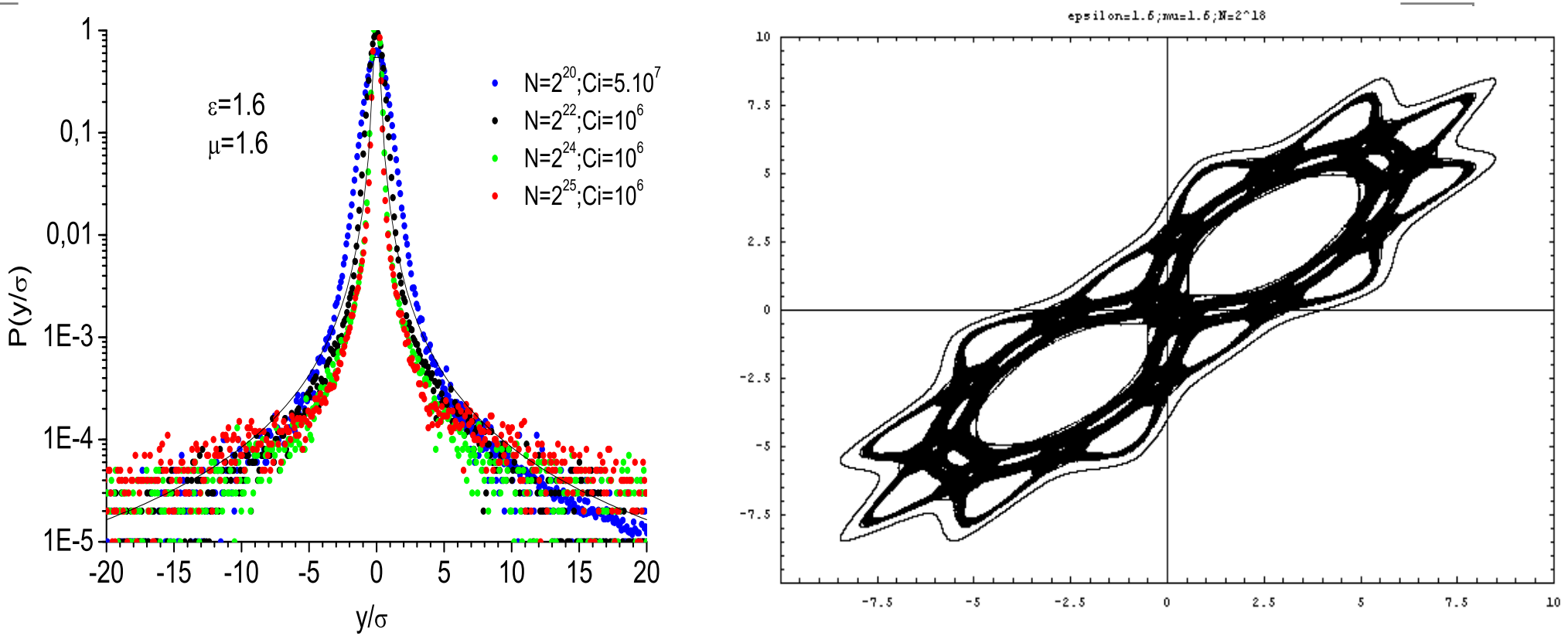

Figure 7. Similar dynamical and statistical behavior of chaotic orbits of the MacMillan map is observed for $\mu = 1.6$, $\epsilon = 1.6$, as in the $\epsilon = 1.2$ case. Orbital diffusion to an outer chain of islands generates pdfs of iterate sums that also converge to a true q–Gaussian as N increases to larger and larger values.

Quasi–stationary Chaotic States in Fermi–Pasta–Ulam Hamiltonians

The FPU $\beta-$ model is a one–dimensional lattice of nonlinear oscillators described by the Hamiltonian

$$H = \frac{1}{2}\sum_{j=1}^{N} p_j^2 + \sum_{j=0}^{N}\left(\frac{1}{2}(q_{j+1}-q_j)^2 + \frac{1}{4}\beta(q_{j+1}-q_j)^4\right) = E \qquad (23)$$

E being its total energy. We shall impose **fixed boundary conditions (fbc)**:
$q_0(t) = q_{N+1}(t) = 0$, or **periodic boundary conditions (pbc)**
$q_j(t) = q_{j+N}(t), \quad p_j(t) = p_{j+N}(t)$, for all $t > 0$.

We focus on **Simple Periodic Orbits (SPOs)**, where all variables oscillate in or out of phase and return to their initial state after only one maximum and one minimum in their oscillation. Examples of such SPOs are **Nonlinear Normal Modes (NNMs)**, i.e. continuations of linear normal modes of the FPU chain described by the Q_q and P_q variables:

$$Q_q = \sqrt{\frac{2}{N+1}}\sum_{i=1}^{N} q_i \sin\frac{qi\pi}{N+1}, \qquad P_q = \dot{Q}_q \qquad (24)$$

These solutions are:

(a) The FPU π–Mode under pbc with N even

$$\hat{q}_j(t) = -\hat{q}_{j+1}(t) \equiv q(t),\ j = 1, \ldots, N \tag{25}$$

(b) The SPO1 mode under fbc, with N odd,

$$\hat{q}_{2j}(t) = 0,\ \hat{q}_{2j-1}(t) = -\hat{q}_{2j+1}(t) \equiv \hat{q}(t),\ j = 1, \ldots, \frac{N-1}{2}. \tag{26}$$

(c) The SPO2 mode under fbc, with $N = 5 + 3m,\ m = 0, 1, 2, \ldots$

$$\hat{q}_{3j}(t) = 0,\ j = 1, 2, 3 \ldots, \frac{N-2}{3}, \tag{27}$$

$$\hat{q}_j(t) = -\hat{q}_{j+1}(t) = \hat{q}(t),\ j = 1, 4, 7, \ldots, N-1. \tag{28}$$

which are exact continuations of the $q = N/2$, $q = (N+1)/2$ and $q = 2(N+1)/3$ linear modes respectively. Let us see what these solutions look like for some small particle chains.

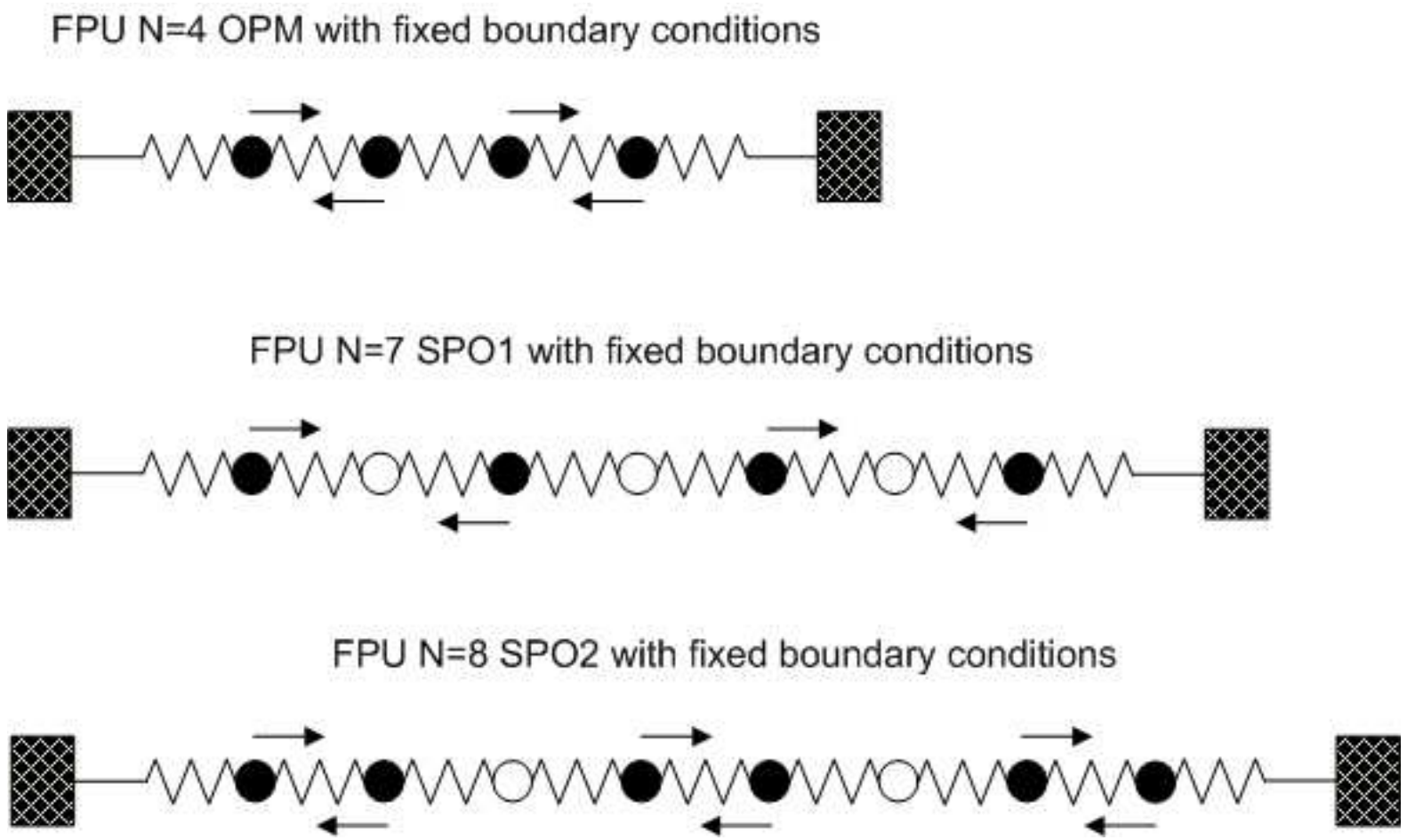

Figure 8: The π–mode of oppositely moving particles, the SPO1 mode corresponding to every other particle being stationary and the SPO2 mode, with one stationary particle every other two.

Our aim is to study chaotic regions near these NNM orbits, when they have just turned unstable.

(a) The FPU π–Mode under pbc with N even
Here, we choose as an observable the quantity

$$\eta(t) = q_{\frac{N}{2}}(t) + q_{\frac{N}{2}-1}(t) \tag{29}$$

using the fact that $\eta(t) = 0$ at energy values E where the π–mode is still stable. At energies above its first destabilization threshold, i.e. $E > E_u^1$, $\eta(t)$ deviates from zero and **starts to explore a thin chaotic layer**. We first consider the case of $N = 128$ and $\beta = 1$ for which $E_u^1 \approx 0.0257$ and take as our total energy $E = 0.768$, at which the π–mode is unstable.

As we see in Figures 9 and 10, when we increase the total integration time of our numerical trajectory, the statistical distributions (red curves) approaching **closer and closer to a Gaussian** with q tending to 1.

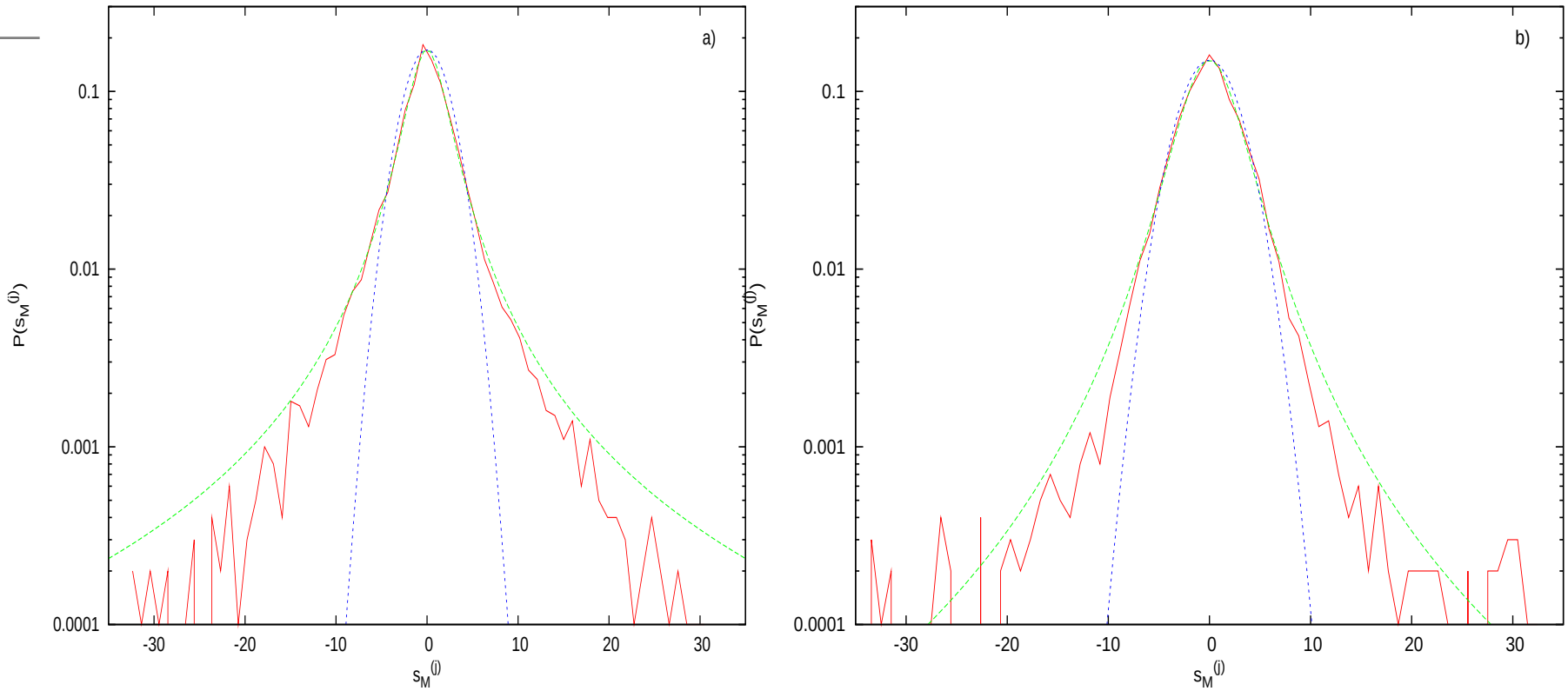

Figure 9. Plot in linear–log scale of numerical (red curve), q–Gaussian (green curve) and Gaussian (blue curve) distributions for the FPU $\pi-$ mode with p.b.c. for $N = 128$ degrees of freedom, $\beta = 1$ and $E = 0.768$. Panel a) corresponds to integration **time** $t_f = 10^5$ using $N_{\text{ic}} = 10$ and $M = 10$ terms in the sums. The numerical fitting with a **q–Gaussian gives** $q \approx 1.818$ with $\chi^2 \approx 0.00070$. Panel b) corresponds to $t_f = 10^6$ using $N_{\text{ic}} = 100$ and $M = 100$ terms in the sums. Here the fitting is with a **q–Gaussian with** $q \approx 1.531$ and $\chi^2 \approx 0.00039$.

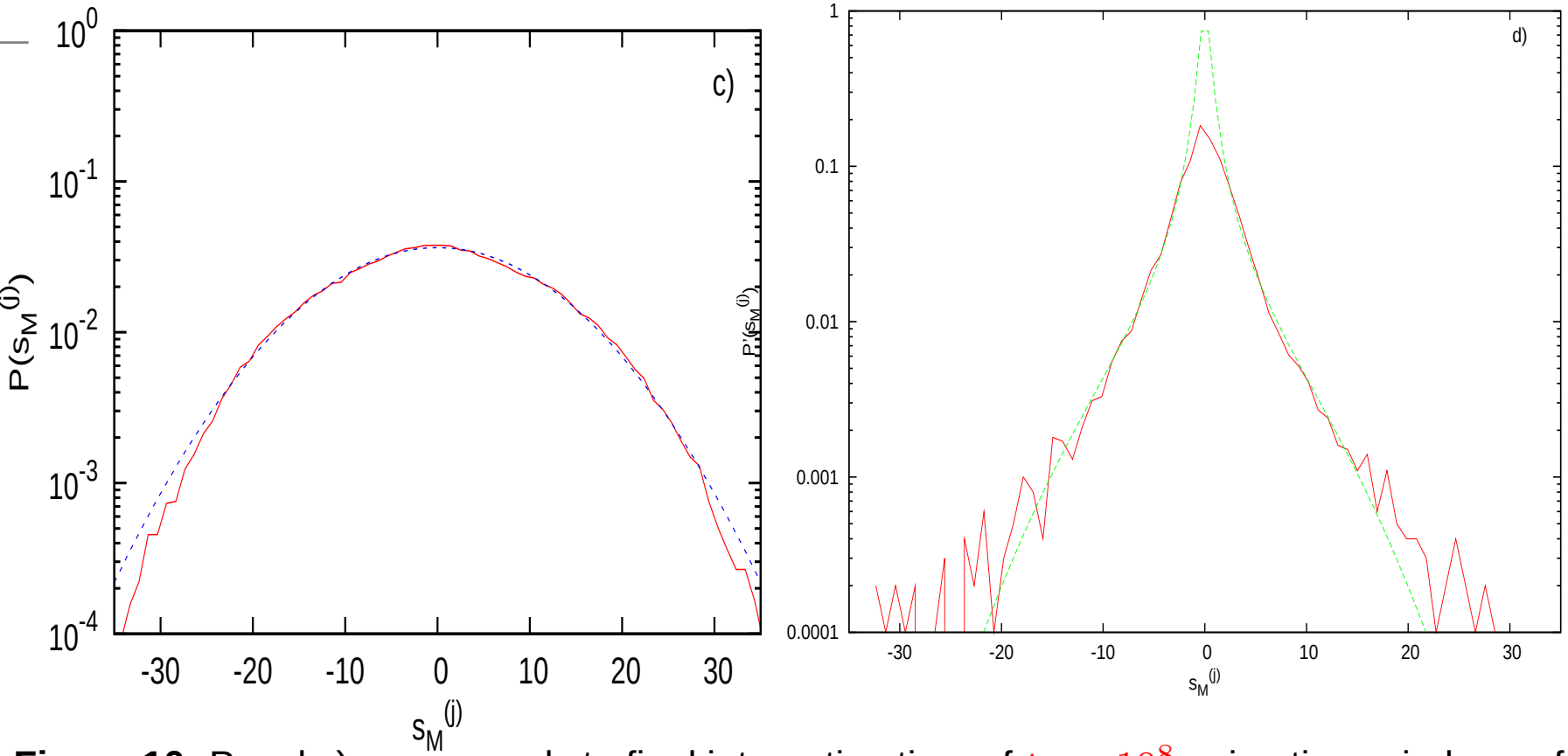

Figure 10. Panel c) corresponds to final integration time of $t_f = 10^8$ using time windows of length $N_{\text{ic}} = 1000$ and $M = 1000$ terms in the computations of the sums. Here the numerical distribution (red curve) has almost converged to a Gaussian (blue curve). Panel d) Plot in linear–log scale of the same numerical distribution as in panel a) (red curve) and of **the P' function of Eq.** (30) for $a_1 \approx 0.009, a_q \approx 2.849$ and $q \approx 2.179$ with $\chi^2 \approx 0.00008$ (green curve). The fitting by this function is evidently better than that with a q–Gaussian.

As Figure 10 (d) shows, the computed distribution (red curve) on its way to a Gaussian, may pass through intermediate QSS, where it is better fitted by a function presented in [Tsallis and Tirnakli, 2010]

$$P'(s_M^{(j)}) = \frac{1}{\left(1 - \frac{a_q}{a_1} + \frac{a_q}{a_1} e^{(q-1)a_1 s_M^{(j)2}}\right)^{\frac{1}{q-1}}}, \; a_1, a_q \geq 0 \text{ and } q > 1 \qquad (30)$$

where $a_1 \approx 0.009, a_q \approx 2.849$ and $q \approx 2.179$ getting $\chi^2 \approx 0.00008$ (in contrast to the $\chi^2 \approx 0.00070$ of a q–Gaussian (14) fitting with $q \approx 1.818$). Eq. (30) contains q–Gaussians in the limit of q being close to 1.

(b) FPU SPO1 mode under fbc

Let us now pass to the second example we consider in this study and examine the chaotic dynamics near another NNM of the FPU system, imposing this time **fixed boundary conditions**. In particular, we study statistical distributions of chaotic orbits in the neighborhood of a nonlinear mode we have called SPO1.

More specifically, we consider the FPU–β one–dimensional lattice of $N = 5$ particles under fbc.

The chaotic regions near this solution (when it has just become unstable) are embedded into each other, as shown in Figure 11. At first, **a "figure eight"** appears created by an orbit starting at a distance $\approx 1.192 \times 10^{-7}$ from the SPO1 mode, see the surface of section (q_1, p_1) of Figure 11 (at times when $q_3 = 0$ and $E = 7.4$).

Orbits starting in the neighborhood of this point remain nearby for very long times, forming the "figure eight" at the middle of the picture. Starting, however, at a distance $\approx 1.086 \times 10^{-2}$ from the saddle point, a **more extended chaotic region** is observed, in the form of a small "figure eight cloud" enveloping the first orbit.

Choosing even more distant initial conditions, e.g. one starting $\approx 3.421 \times 10^{-1}$ from the saddle point, a **much larger chaotic region** is obtained, which spreads uniformly over a much larger part of the available energy surface.

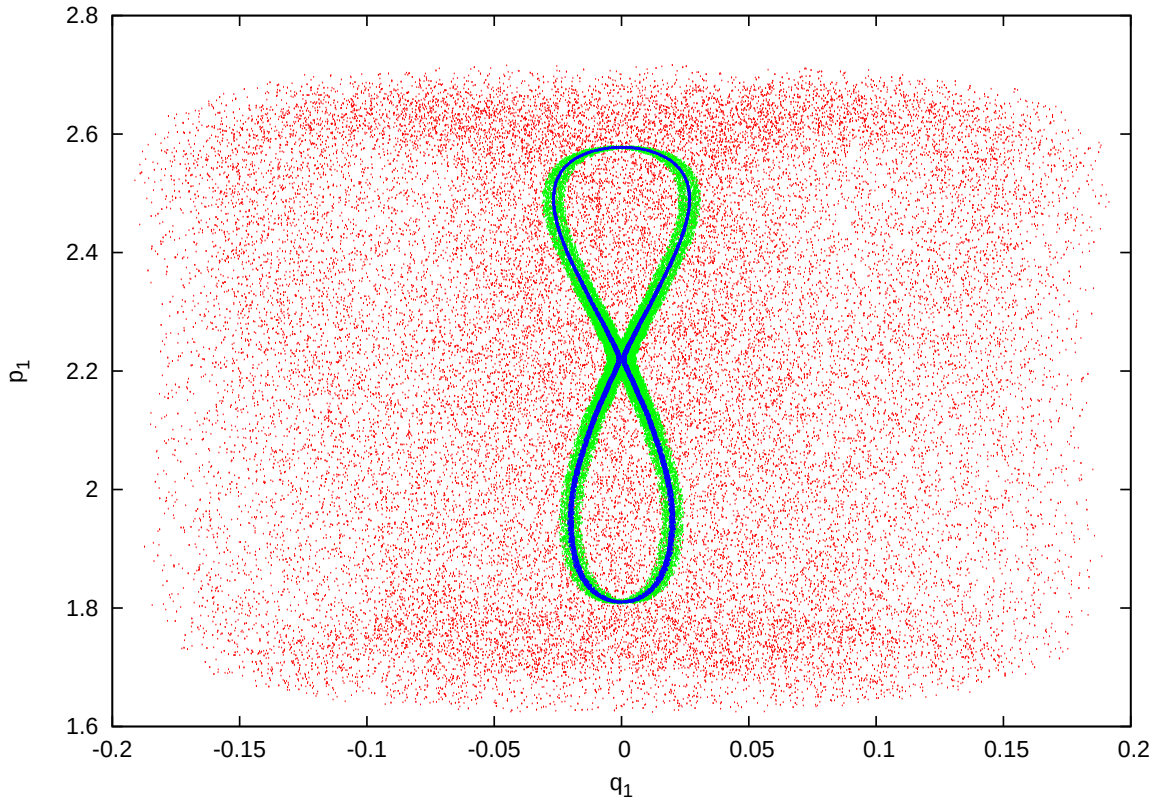

Figure 11: (i) The "figure eight" chaotic region (blue points) for an orbit starting at a distance $\approx 1.192 \times 10^{-7}$ from SPO1 mode at the saddle point in the figure), (ii) a fatter "figure eight cloud" (green points) is seen starting at ($\approx 1.086 \times 10^{-2}$) and a much larger chaotic region (red points) on the energy surface for an initial condition even more distant ($\approx 3.421 \times 10^{-1}$). $N = 5$ and $\beta = 1$, on the surface of section (q_1, p_1) computed at $q_3 = 0$. In this figure, we have integrated our three orbits up to $t_f = 10^5$ on the energy surface $E = 7.4$.

In the present example, we have chosen as an observable the quantity

$$\eta(t) = q_1(t) + q_3(t) \tag{31}$$

which is equal to zero at the SPO1 orbit and becomes nonzero due to numerical errors at energies just above the first destabilization energy E_u^1 of the mode.

We may study 3 different initial conditions located on the neighborhood of the unstable SPO1 mode (see Fig. 11). Equivalently, in Figures 12, 13 and 14, we plot on the left panel the surface of section (of the trajectory starting at $\approx 1.192 \times 10^{-7}$ from the unstable SPO1) **for times $t_f = 10^5$, $t_f = 10^7$ and $t_f = 10^8$ respectively**, while on the right panels we plot the corresponding pfds of the normalized sums.

Clearly, as the integration time t_f grows, our chaotic orbit eventually wanders over a more extended domain, covering gradually a much larger part of the energy surface when $t_f = 10^8$. This may also be explained by the behavior of the Lyapunov exponents of the orbit (see Figure 15).

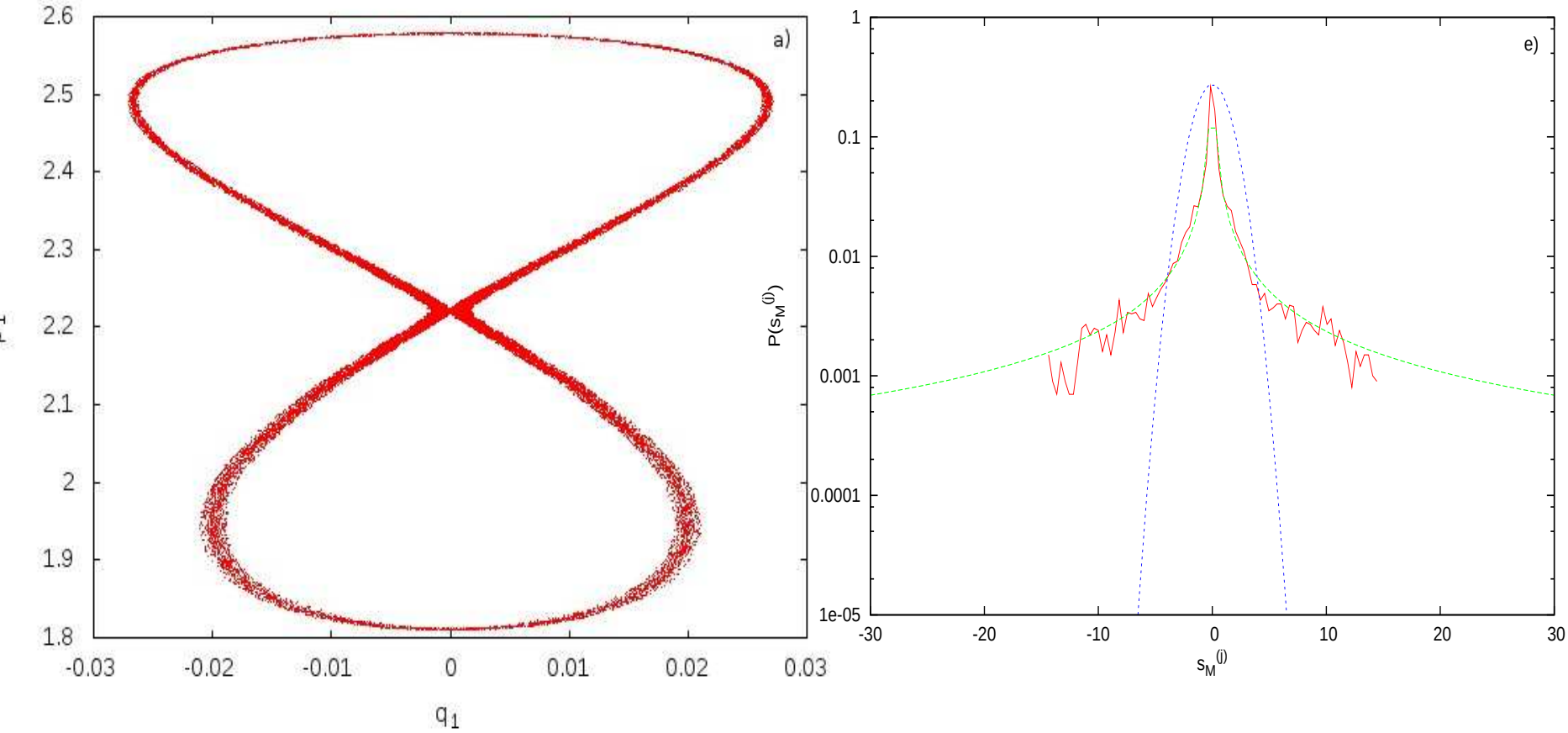

Figure 12. Left: Surface of section of a trajectory starting from a distance of $\approx 1.192 \times 10^{-7}$ from the unstable SPO1 saddle and integrated for **a total time** $t_f = 10^5$. **Right:** For the same integration time, we find that the pdf representing the **distribution of the sums** is well fitted by a q**–Gaussian,** $q \approx 2.785$ with $\chi^2 \approx 4.05 \times 10^{-6}$.

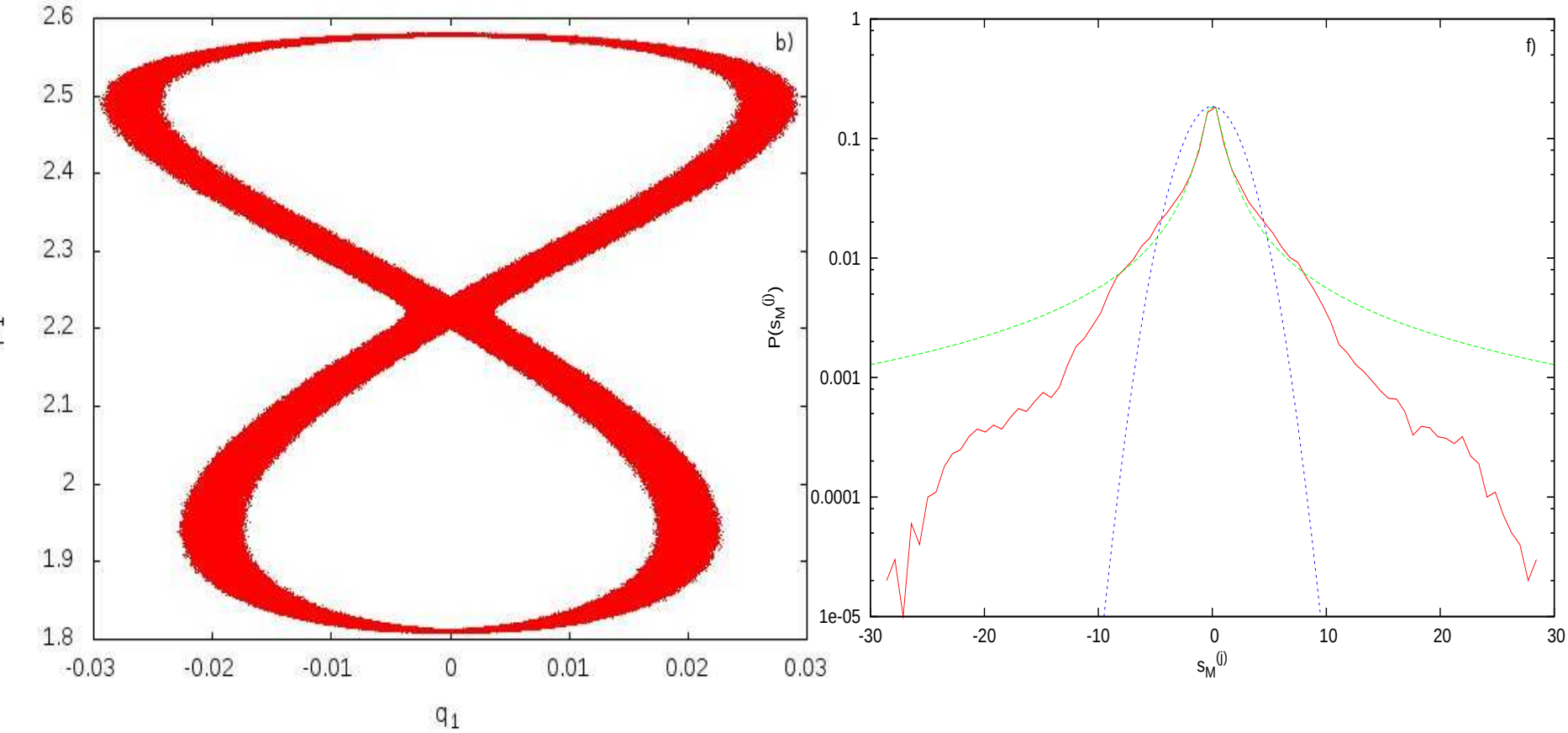

Figure 13: Left: Surface of section of a trajectory starting from a distance $\approx 1.192 \times 10^{-7}$ from the unstable SPO1 saddle point total after time $t_f = 10^7$. **Right:** For the same integration time, the **statistical distribution of the sums** of one chaotic component of the orbit can still be fitted–but not as well–by a q**–Gaussian with** $q \approx 2.483$ with $\chi^2 \approx 6.05 \times 10^{-6}$.

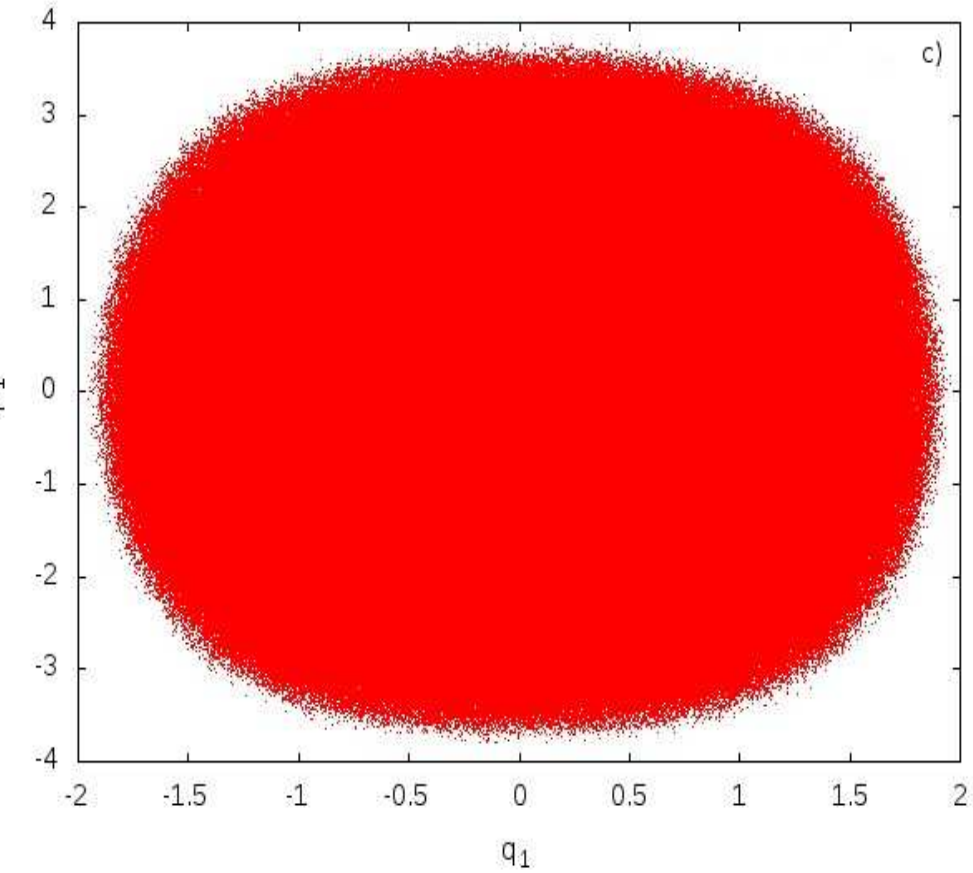

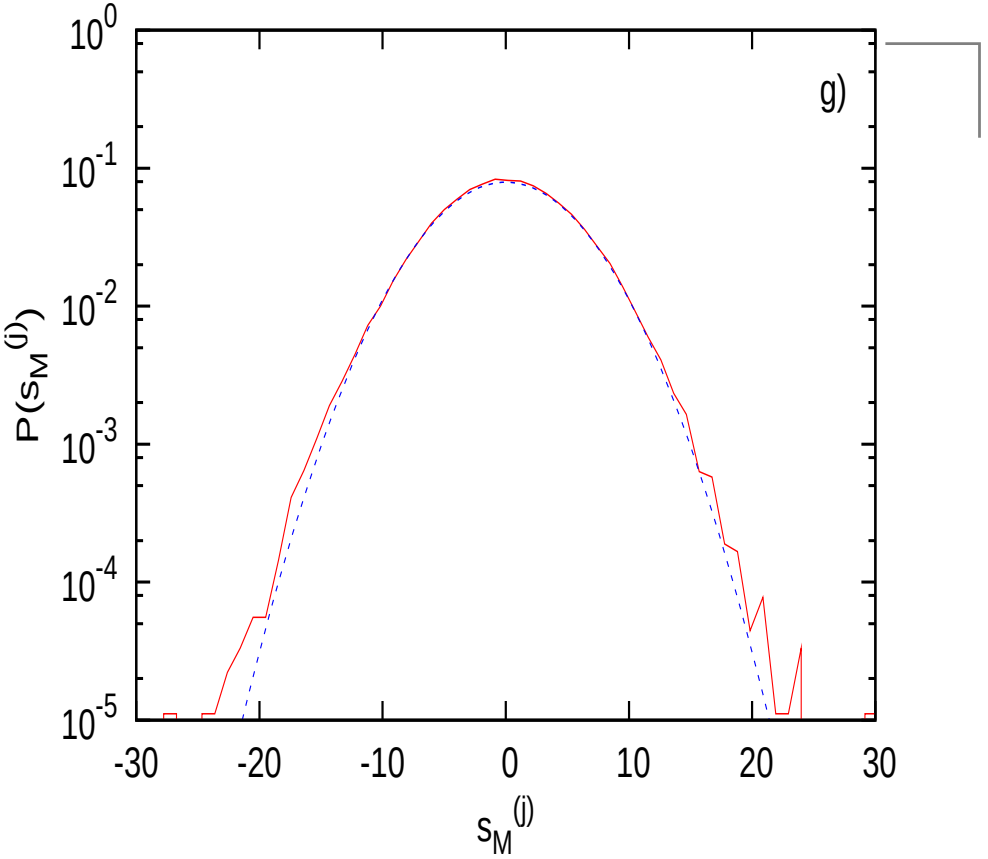

Figure 14: Left: Surface of section of the same trajectory for **total integration time** $t_f = 10^8$. **Right:** Final integration time $t_f = 10^8$ in the computations of the sums. In this case it is evident that **the distribution appears to converge to a Gaussian (q=1)**.

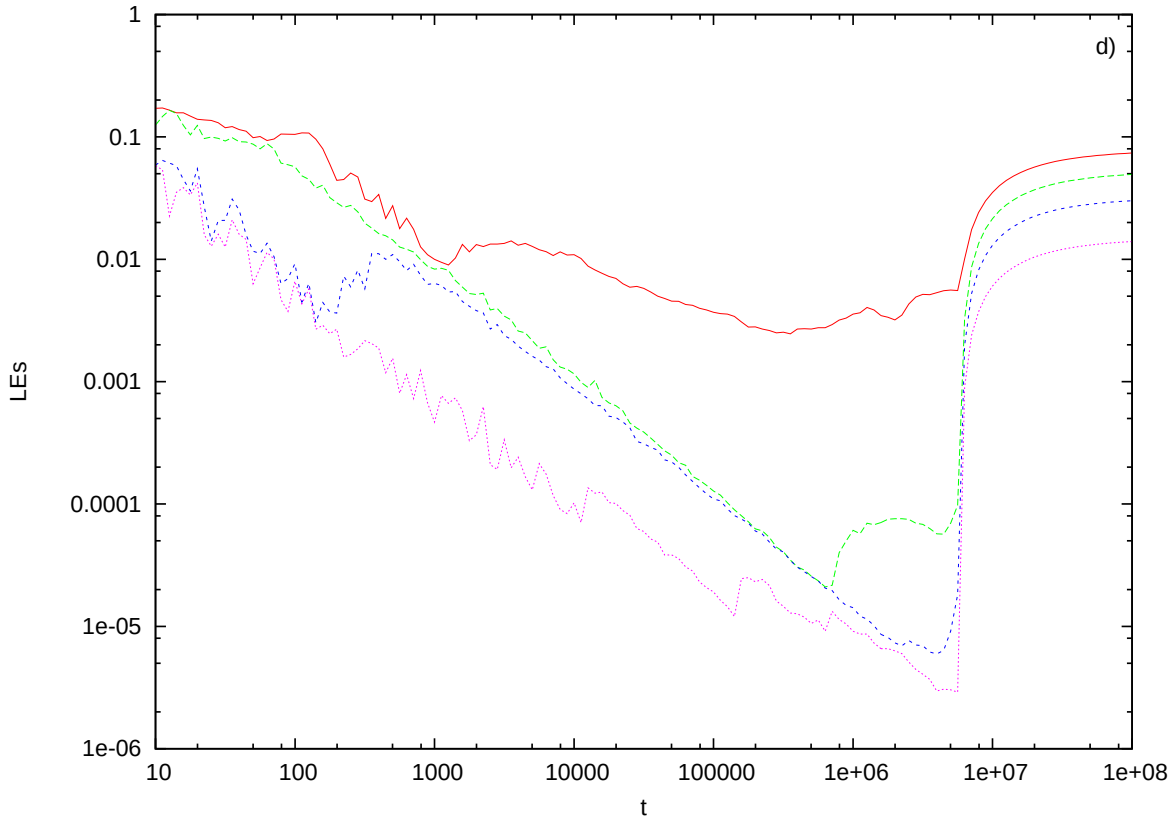

Figure 15: The 4 positive Lyapunov exponents of the previous solution integrated for a total time of $t = 10^8$. Observe the **sudden jump in their magnitude at ($t \simeq 10^7$)**, where the orbit **escapes from the region of "weak chaos" and q–Gaussian distributions** into the wider chaotic domain of **"strong chaos" where the statistics is Gaussian**.

(c) FPU SPO2 mode under fbc

We also examined the neighborhood of the SPO2 mode, which becomes unstable at much smaller energies. Thus, we expect that, near SPO2, orbits will be more weakly chaotic and QSS will persist for longer times.

As figure 16 shows, orbits now trace out a kind of **"banana" shaped region** (Fig. 16(a)) in a regime of **very small (positive) Lyapunov exponents** (Fig. 16(b)). Here, the normalized sum pdfs, up to $tf = 10^{10}$!, **converge to a function that is close to a q–Gaussian** and never deviates towards a Gaussian. As we see in Figure 16(a), the dynamics near SPO2 **"sticks" to a type of quasiperiodic torus**, at least up to $t_f = 10^8$.

In Figure 16(b), we have plotted the four positive Lyapunov exponents up to $t_f = 10^9$. Note that, although they are all seen to decrease towards zero, at about $t_f > 10^9$, **the largest exponent shows a tendency to converge to a very small value of about 10^{-7}**, indicating that the orbit is chaotic and "sticky" to some quasiperiodic torus near SPO2.

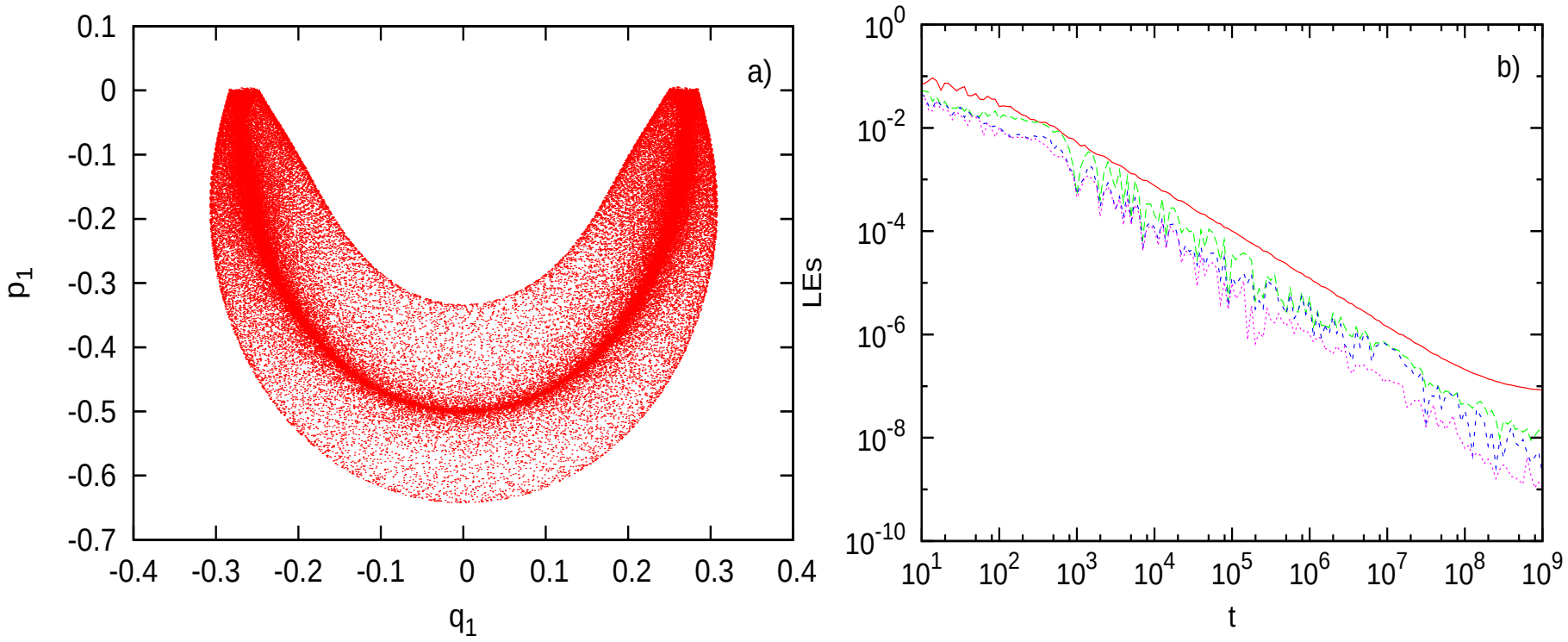

Figure 16: (a) The dynamics near SPO2 "sticks" to a quasiperiodic banana–like state, at least up to $t_f = 10^8$. The weakly chaotic nature of the motion is shown in (b), where we have plotted the four positive Lyapunov exponents up to $t_f = 10^9$. Note that, although they all decrease towards zero, at about $t_f > 10^9$, **the largest exponent shows a tendency to converge to a very small value of about** 10^{-7}, indicating that the orbit is chaotic.

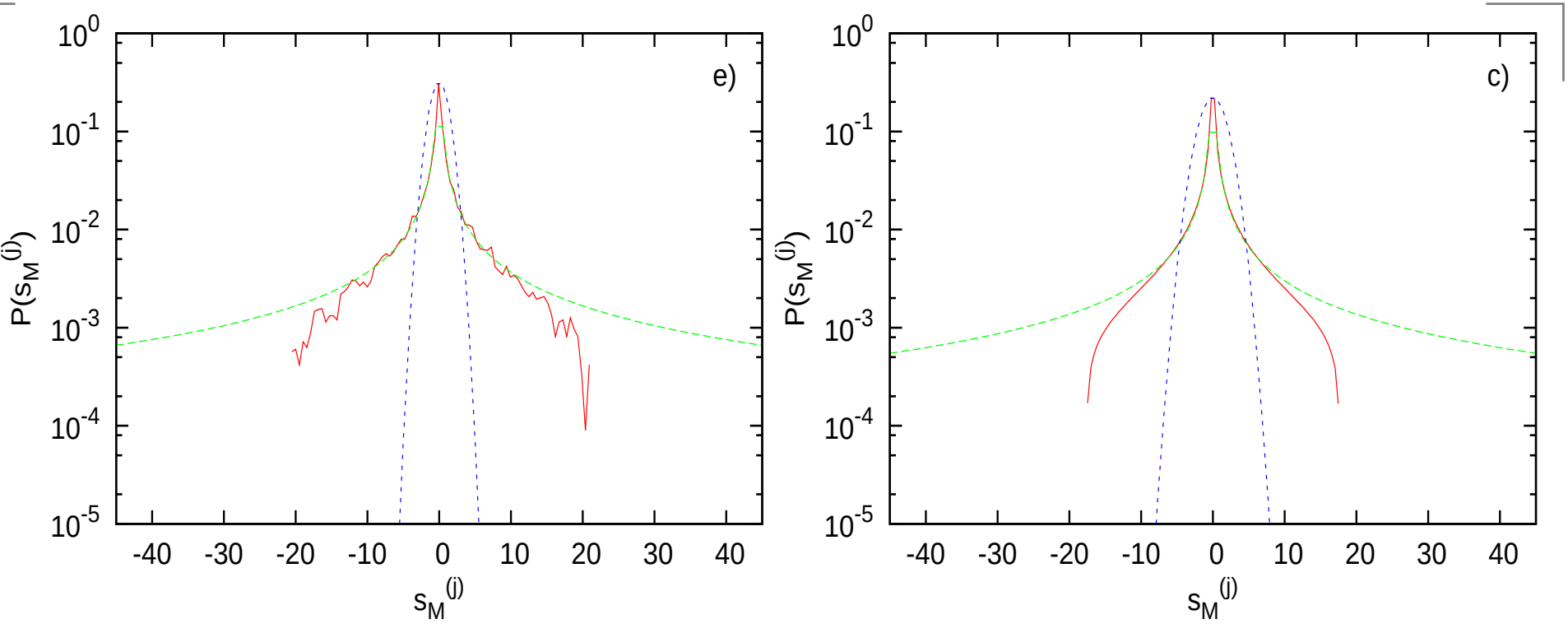

Figure 17: Left panel: The distribution of the normalized sum pdf of the orbit starting near SPO2, for a total integration time $t_f = 10^6$. Right panel: Final integration time $t_f = 10^{10}$ the normalized sum pdf has converged to a shape that closely resembles a q–Gaussian with $q \approx 2.769$ and $\chi^2 \approx 4.44 \times 10^{-5}$.

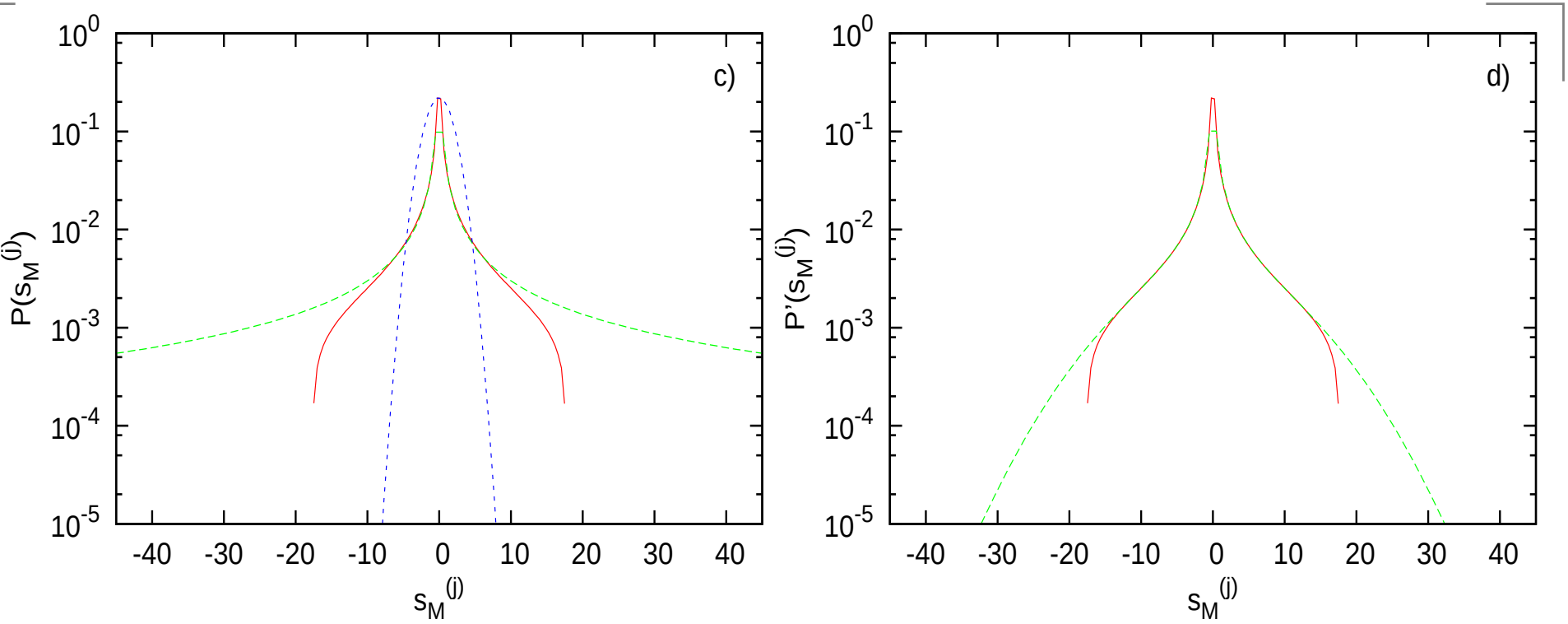

Figure 18: Left panel: The converged distribution of the normalized sum pdf of the orbit starting near SPO2, for $t_f = 10^{10}$. Right panel: Its analytical form is better approximated by the crossover formula (30)where $a_1 \approx 0.006$, $a_q \approx 170$ and $q \approx 2.82$ with $\chi^2 \approx 2.06 \times 10^{-6}$, than a q–Gaussian with $q \approx 2.769$ and $\chi^2 \approx 4.44 \times 10^{-5}$.

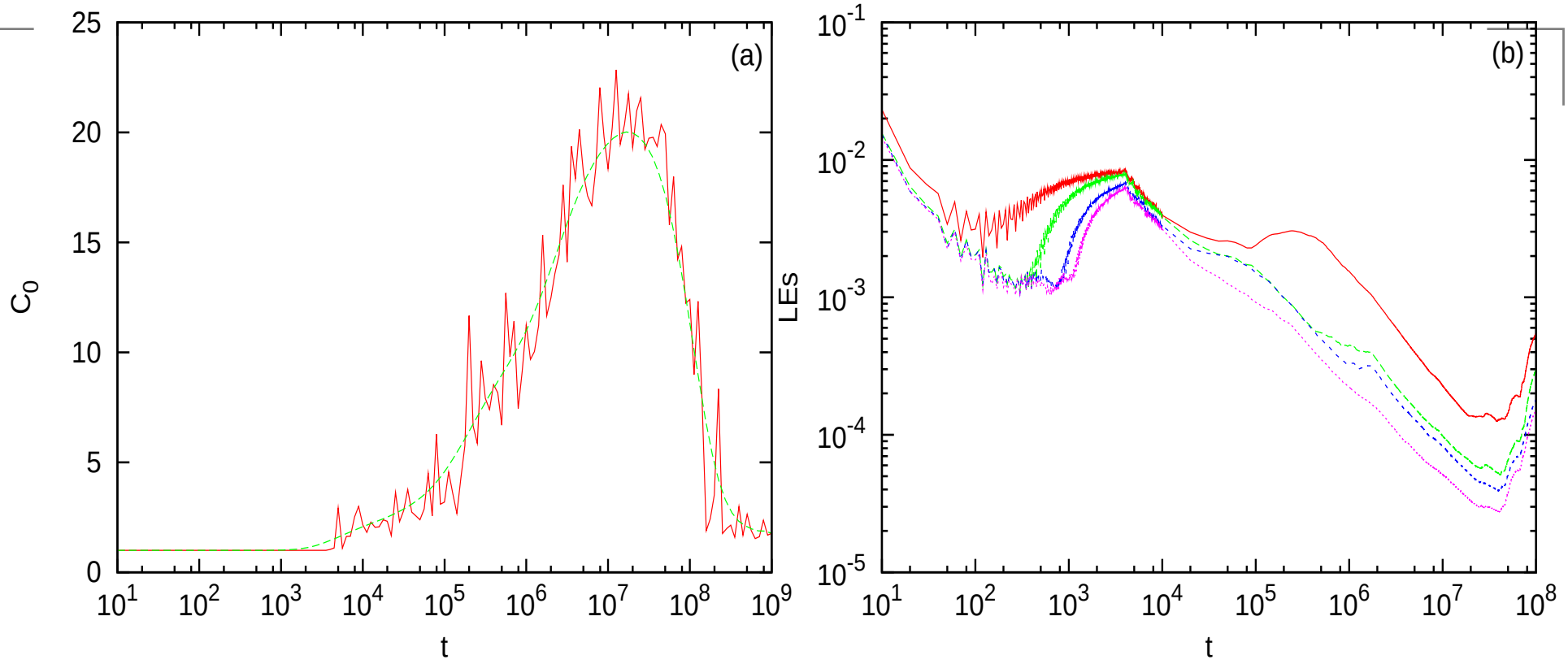

Figure 19: Left Panel: Plot of the sum average of squared energies of each site $C_0(t)$ as a function of time for the unstable ($E = 0.768 > E_u \approx 0.0257$) π-mode with $\beta = 1$ and $N = 128$. **Right Panel:** Log-log plot of the four biggest Lyapunov exponents as a function of time for the same parameters as in panel (a).

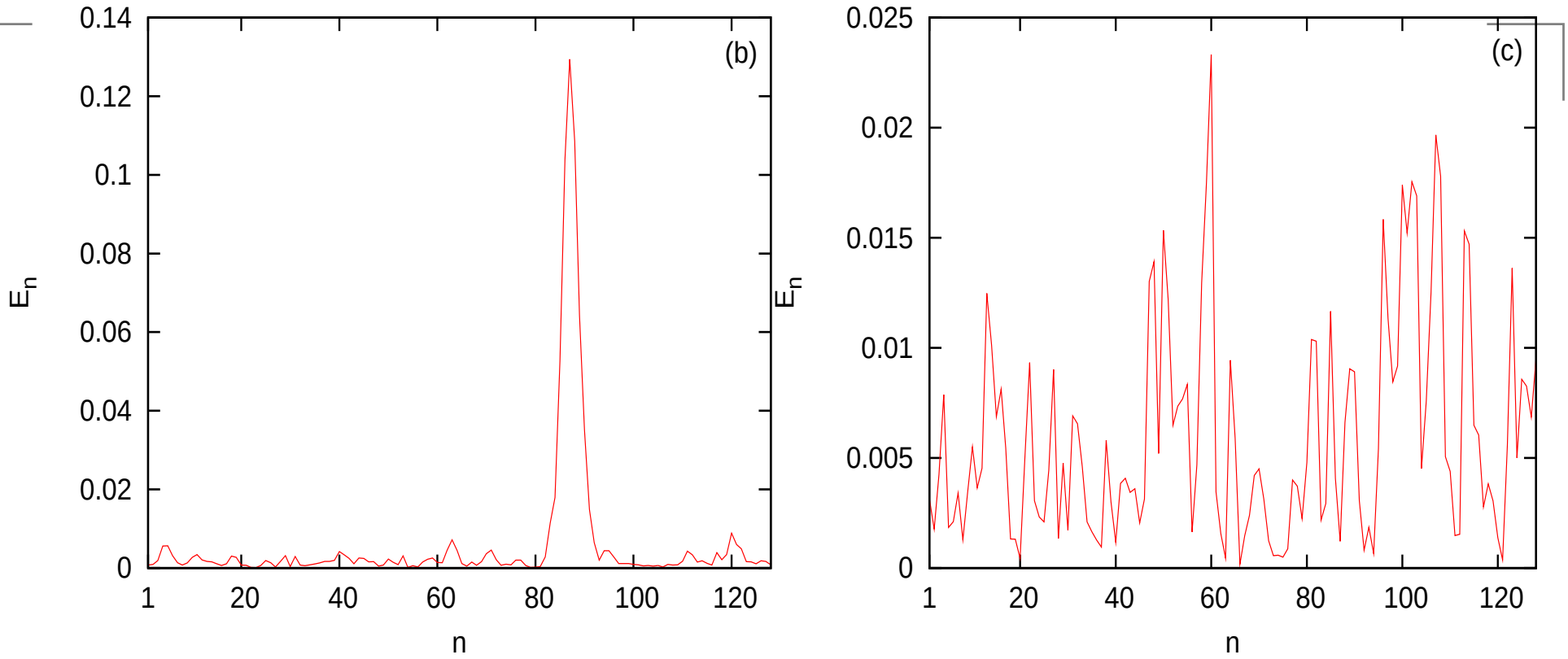

Figure 20: Left Panel: Plot of the instantaneous on site energy $E_n = \frac{1}{2}p_n^2 + \frac{1}{2}V(q_{n+1} - q_n) + \frac{1}{2}V(q_n - q_{n-1})$ along the $N = 128$ FPU chain with p.b.c., at time $t = 9 \times 10^7$ (observation of a **chaotic breather**), where the corresponding pdf is a q-Gaussian (q>1). **Right Panel:** At time $t = 6 \times 10^8$, **the chaotic breather has collapsed**, energy equipartition has occurred and the pdf tends to a true Gaussian.

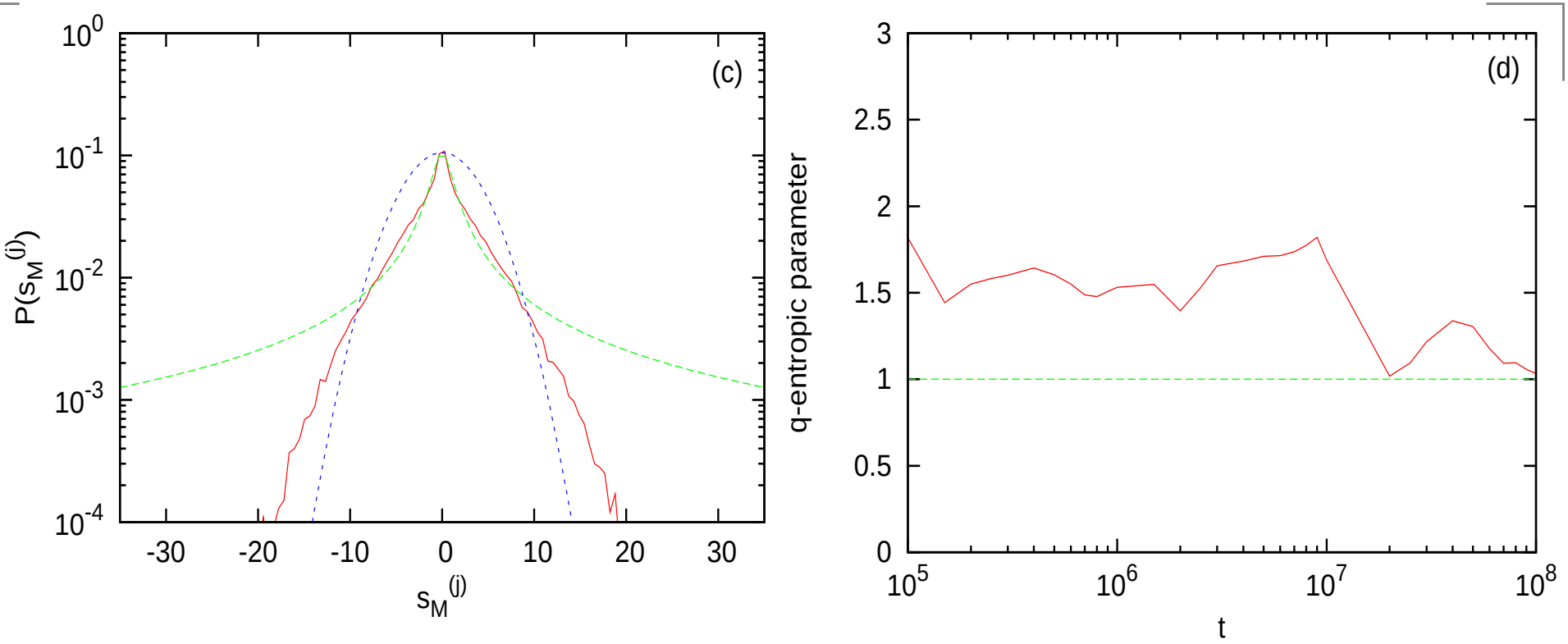

Figure 21: Left Panel: At $t = 10^7$, the sum distribution, near the maximum of the chaotic breather, is still quite close to a q-Gaussian with $q \approx 1.6$.**Right Panel:** presents an estimate of the q index at different times, which shows that its values on the average fall significantly closer to 1 for $t > 10^7$.

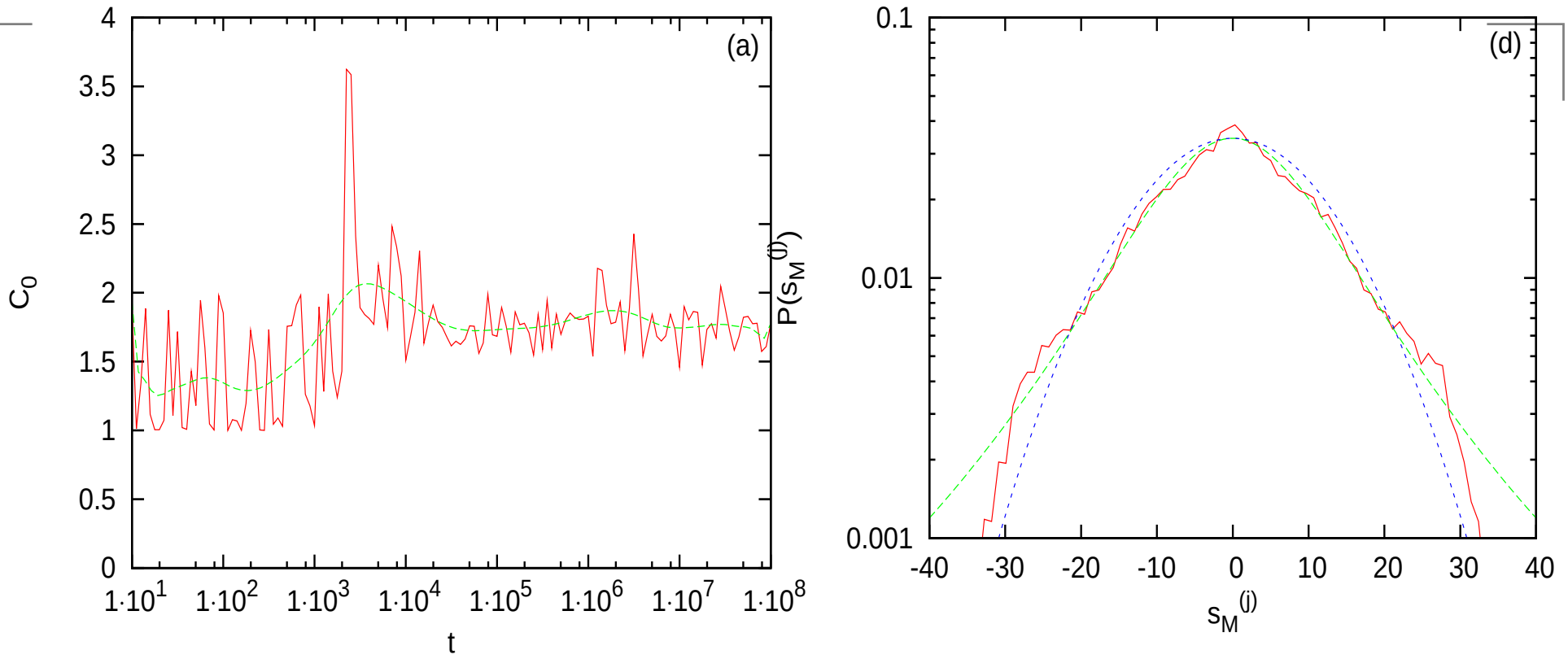

Figure 22: Left Panel: Plot of C_0 as a function of time for a perturbation of the unstable ($E = 1.5 > E_u^{\text{SPO1}} \approx 1.05226$) SPO1 mode with $\beta = 1.04$ and $N = 129$ at initial distance 2.22×10^{-7}. **Right Panel:** Plot in linear-log scale of numerical (red curve), q-Gaussian (green curve) and Gaussian (blue curve) distributions, after time $t_{\mathbf{f}} = 2 \times 10^6$, with $N_{\text{ic}} = 5 \times 10^4$ and $M = 20$. Here, the numerical fitting gives $q \approx 1.564$ with $\chi^2 \approx 0.00014$.

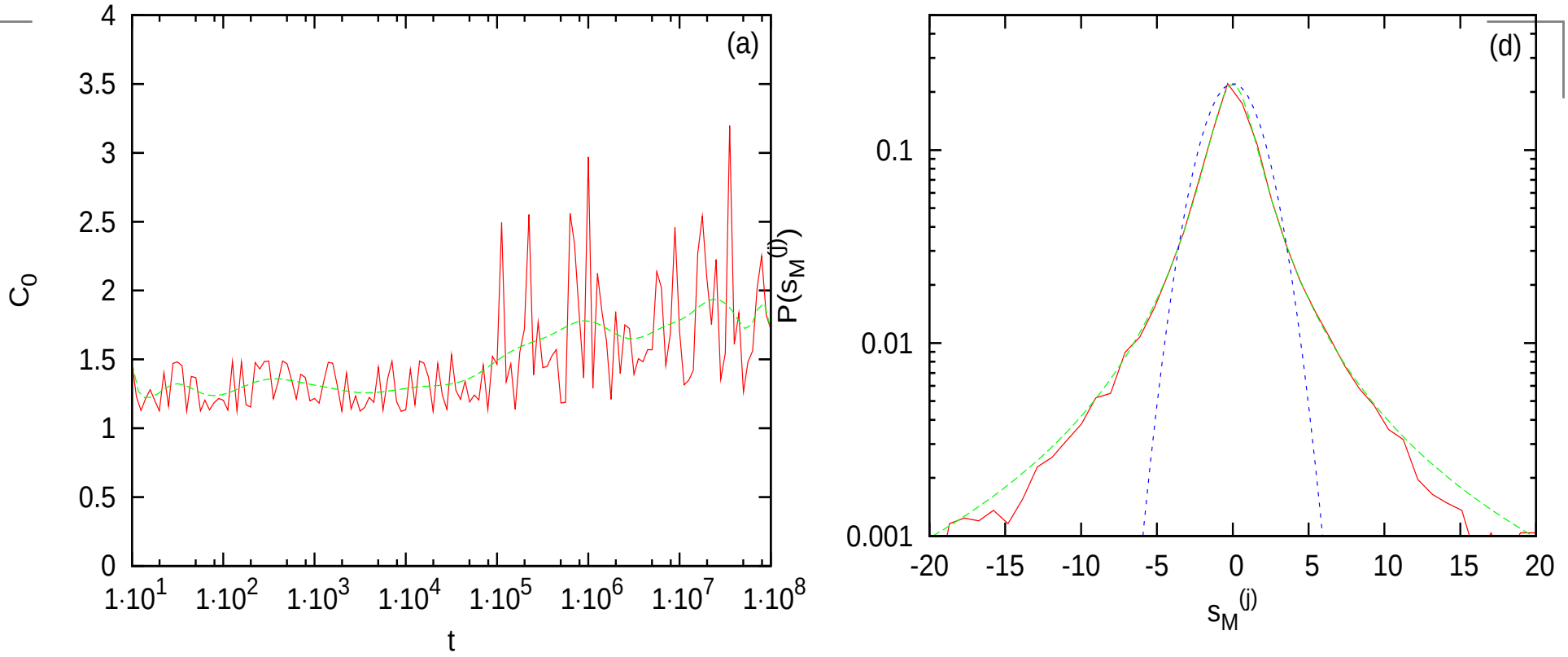

Figure 23: Left Panel: Plot of C_0 as a function of time for a perturbation of the unstable ($E = 0.1 > E_u^{\text{SPO2}} \approx 0.01279$) SPO2 mode with $\beta = 1$ and $N = 128$ at initial distance 4.09×10^{-7}. **Right Panel:** Plot in linear-log scale of numerical (red curve), q-Gaussian (green curve) and Gaussian (blue curve) distributions, after time $t_{\mathbf{f}} = 10^6$, with $N_{\text{ic}} = 2.5 \times 10^4$ and $M = 20$. Here, the numerical fitting gives $q \approx 1.943$ with $\chi^2 \approx 0.00035$.

Weakly and Strongly Chaotic Orbits in a Barred Galaxy Model

The motion of **a test particle in a 3D rotating model of a barred galaxy** is governed by the Hamiltonian:

$$H = \frac{1}{2}(p_x^2 + p_y^2 + p_z^2) + V(x, y, z) - \Omega_b(xp_y - yp_x). \tag{32}$$

The bar rotates around its z–axis (short axis), while the x–direction is along the major axis and the y along the intermediate axis of the bar. Ω_b **is the pattern speed of the bar and** H **is the total energy** of the orbit in the rotating frame of reference (Jacobi constant). The corresponding equations of motion are:

$$\dot{x} = p_x + \Omega_b y, \qquad \dot{y} = p_y - \Omega_b x, \qquad \dot{z} = p_z, \tag{33}$$

$$\dot{p_x} = -\frac{\partial V}{\partial x} + \Omega_b p_y, \qquad \dot{p_y} = -\frac{\partial V}{\partial y} - \Omega_b p_x, \qquad \dot{p_z} = -\frac{\partial V}{\partial z}.$$

The potential V of our model consists of three components: (1) A Miyamoto-Nagai disc:

$$V_D = -\frac{GM_D}{\sqrt{x^2 + y^2 + (A + \sqrt{z^2 + B^2})^2}}. \tag{34}$$

(2) A bulge, modeled by a Plummer sphere whose potential is:

$$V_S = -\frac{GM_S}{\sqrt{x^2+y^2+z^2+\epsilon_s^2}}, \tag{35}$$

where ϵ_s is the scale-length of the bulge and M_S is its total mass.
(3) A triaxial Ferrers bar, with density $\rho(x)$:

$$\rho(x) = \begin{cases} \rho_c(1-m^2)^2 & , m < 1 \\ 0 & , m \geq 1 \end{cases}, \tag{36}$$

where $\rho_c = \frac{105}{32\pi}\frac{GM_B}{abc}$ is the central density, M_B the total mass of the bar and

$$m^2 = \frac{x^2}{a^2} + \frac{y^2}{b^2} + \frac{z^2}{c^2}, \qquad a > b > c > 0, \tag{37}$$

a, b and c being the semi-axes. The corresponding potential is:

$$V_B = -\pi G a b c \frac{\rho_c}{n+1} \int_\lambda^\infty \frac{du}{\Delta(u)} (1 - m^2(u))^{n+1}, \tag{38}$$

where $m^2(u) = \frac{x^2}{a^2+u} + \frac{y^2}{b^2+u} + \frac{z^2}{c^2+u}$, $\Delta^2(u) = (a^2+u)(b^2+u)(c^2+u)$, n is a positive integer (with $n = 2$ for our model) and λ is the unique positive solution of $m^2(\lambda) = 1$, outside of the bar ($m \geq 1$), and $\lambda = 0$ inside the bar. We use the parameter values G=1, Ω_b=0.054 (54 $km \cdot sec^{-1} \cdot kpc^{-1}$), a=6, b =1.5, c=0.6, A=3, B=1, ϵ_s=0.4, M_B=0.1, M_S=0.08, M_D=0.82. The units are: 1 kpc (length), 1000 $km \cdot sec^{-1}$ (velocity), 1 Myr (time), $2 \times 10^{11} M_{\odot}$ (mass). The total mass $G(M_S + M_D + M_B)$ is set equal to 1.

Realistically, the maximal time of integration of the orbits is T=10000Myr (10 billion yrs), corresponding to a time of the order of one Hubble time. **The question therefore is: Can we use pdfs to identify the " weakly" vs. "strongly" chaotic nature of the orbits based only on the small set of data provided by the integration over only** $T = 10000$**?**.

We test first **the 2-degree-of-freedom case:**
1) Strongly Chaotic Orbit 1: $H = E = -0.3$, $(x, y, p_x, p_y) = (0, -0.625, -0.314512, -0.24)$
2) Weakly Chaotic Orbit 2: $H = E = -0.36$, $(x, y, p_x, p_y) = (0, -0.625, -0.002, -0.24)$

and then apply our methods to a more realistic 3-degree-of-freedom example

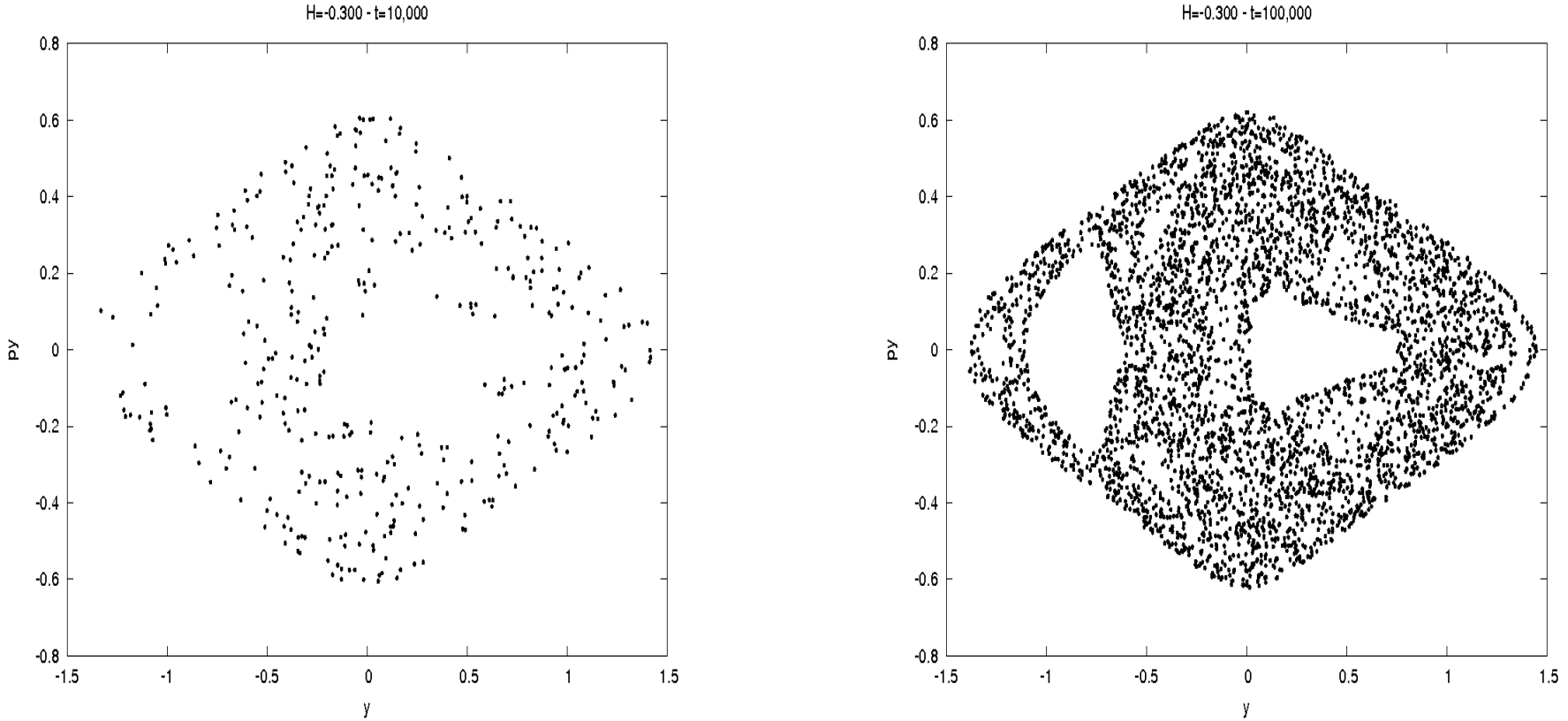

Figure 24: The Poincaré Surface of Section (PSS) (y, p_y) with $p_x > 0,\ x = 0$ for **the Chaotic Orbit 1** above of the 2DOF Hamiltonian system for final integration time $t_f = 10000$ (left panel) and $t_f = 100000$ (right panel) for the same data.

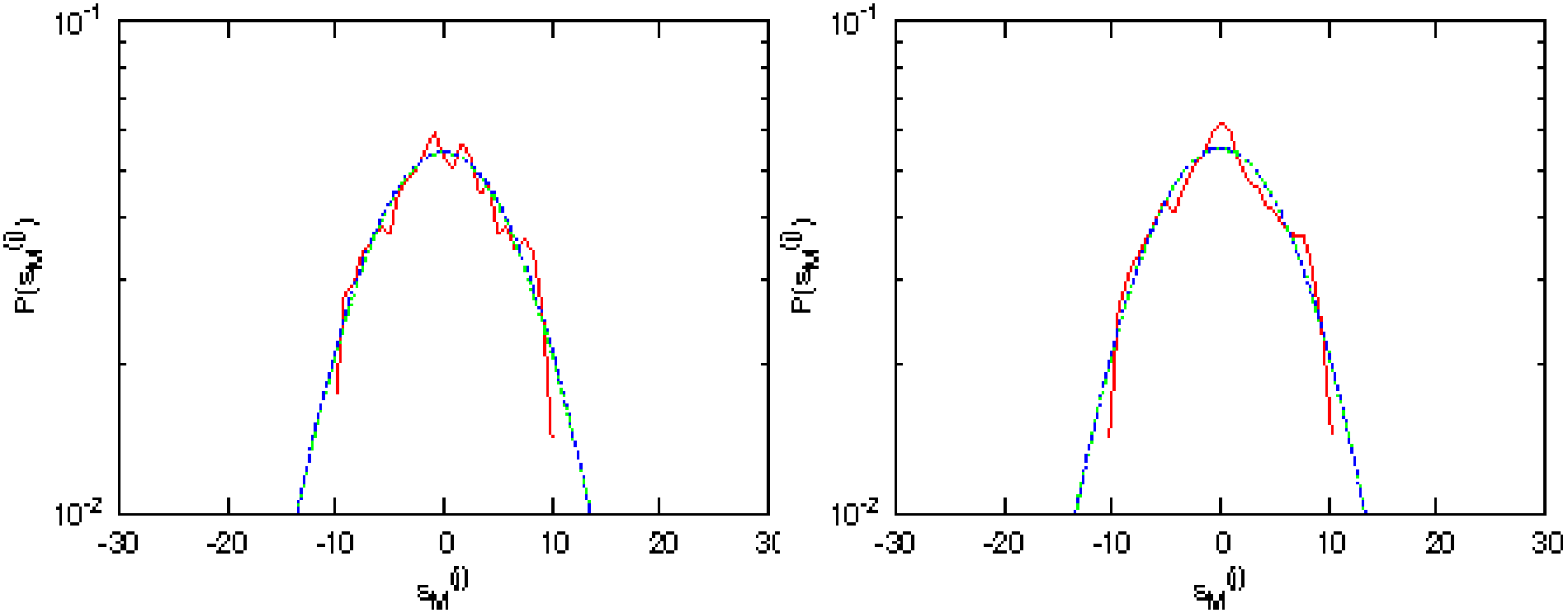

Figure 25: Pdfs of $\eta = x + y$ for the **the Chaotic Orbit 1** above: Plot in linear-log scale of numerical (red curve), q-Gaussian (green curve) and Gaussian (blue curve) distributions. **Left panel: Final integration time** $t_f = 10000$, with $N_{\text{ic}} = 4000$ time windows and $M = 50$ terms in the sums. Numerical fitting with a q-Gaussian gives $q \approx 1.095$ with $\chi^2 \approx 0.0003$. **Right panel:** $t_f = 100000$, $N_{\text{ic}} = 20000$ and $M = 10$, with $q \approx 0.97$ and $\chi^2 \approx 0.00033$.

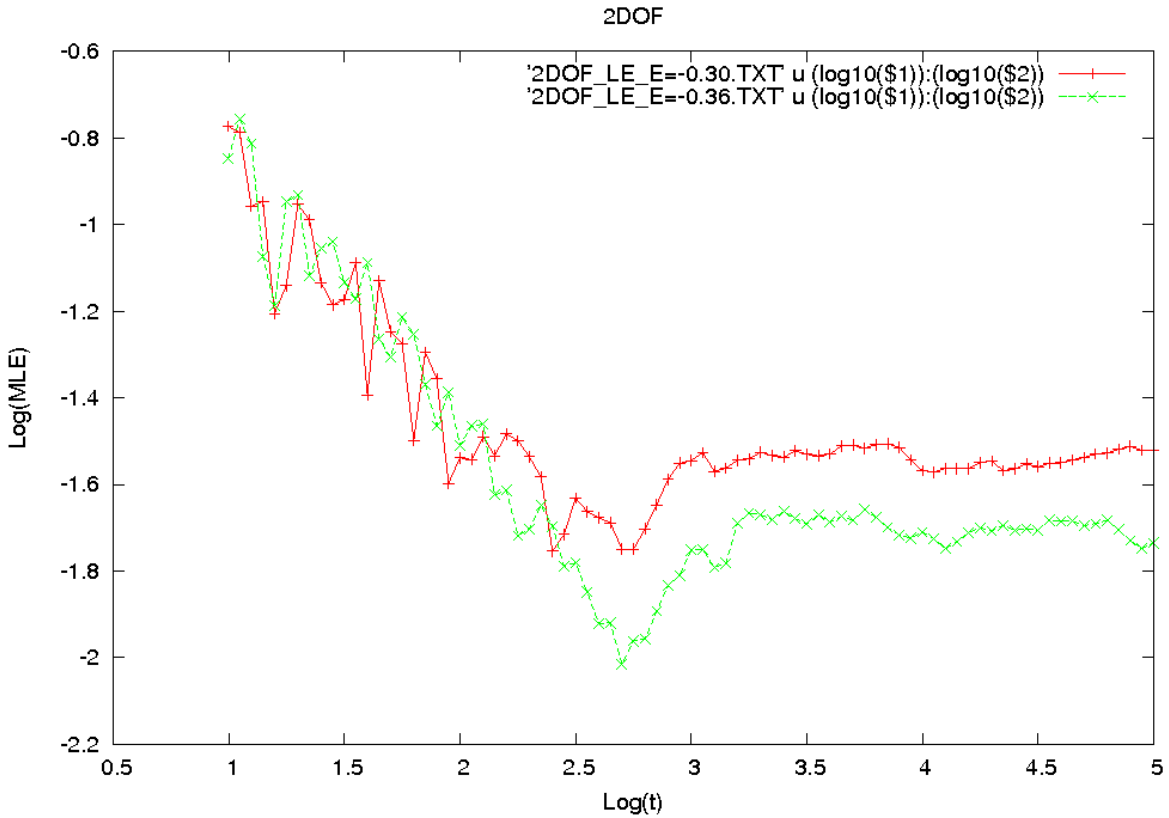

Figure 26: Maximum Lyapunov exponent evolution up to $t_f = 100000$ for the **the Chaotic Orbit 1** of the 2DOF Hamiltonian system (red curve) and for the Weakly Chaotic Orbit 2 of the same system (green curve).

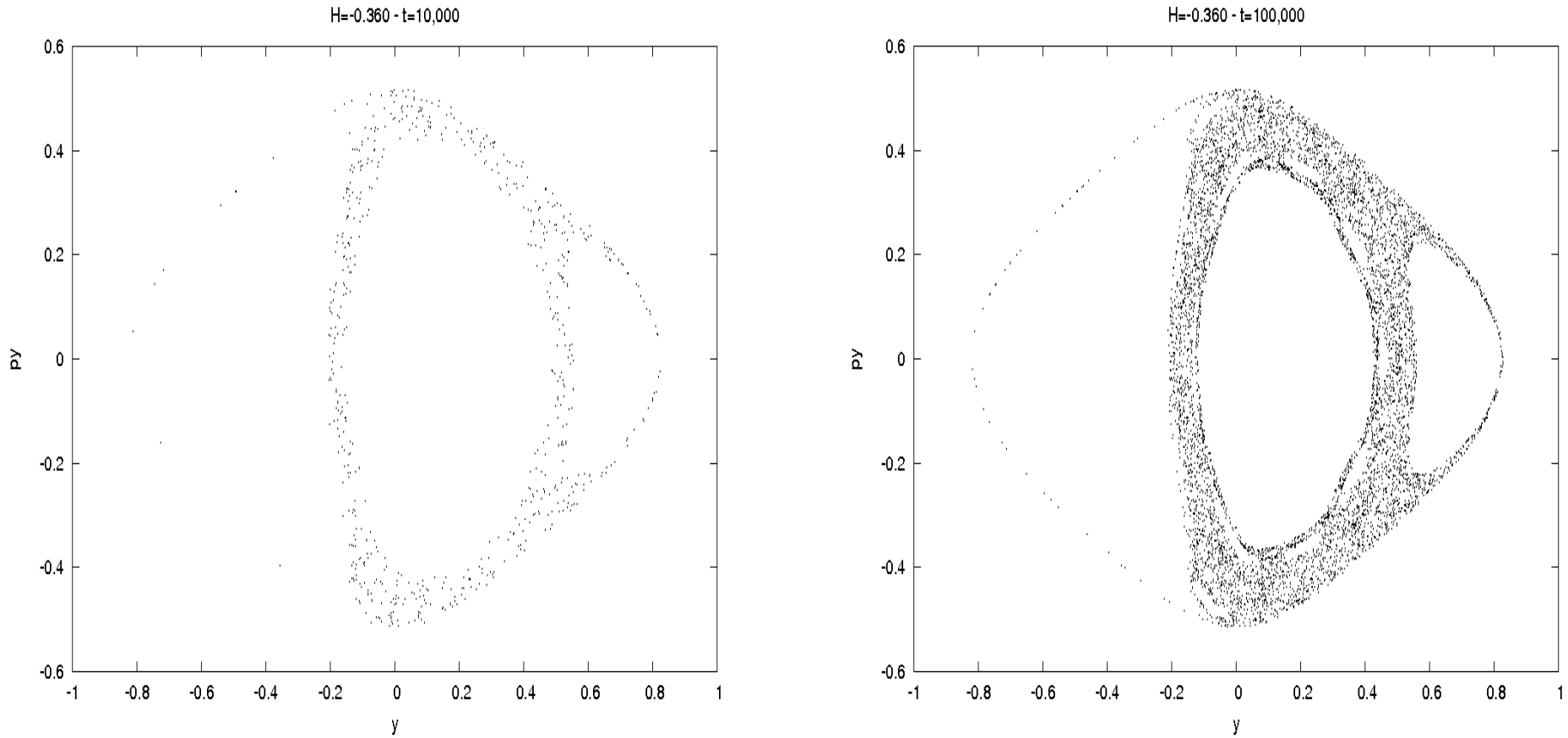

Figure 27: Left panel: The Poincaré Surface of Section (PSS) (y, p_y) with $p_x > 0,\ x = 0$ for the **the Weakly Chaotic Orbit 2** of the 2DOF Hamiltonian system for integration time $t_f = 10000$ **(left panel) and** $t_f = 100000$ **(right panel)** for the same data.

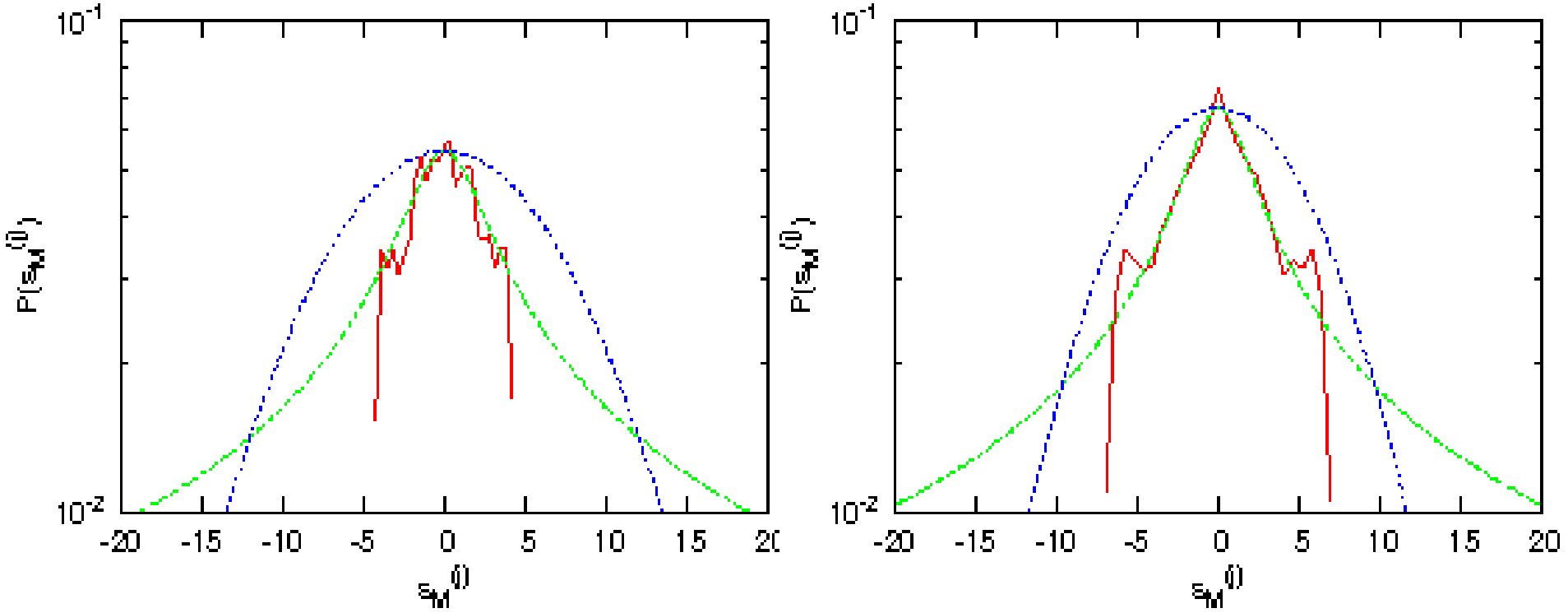

Figure 28: Pdfs of $\eta = x + y$ for the **the Weakly Chaotic Orbit 2**: Plot in linear-log scale of numerical (red curve), q-Gaussian (green curve) and Gaussian (blue curve) distributions.**Left panel: Final integration time** $t_f = 10000$, $N_{\text{ic}} = 4000$ and $M = 50$ terms. Fitting with a q-Gaussian gives $q \approx 3.52$ with $\chi^2 \approx 0.00074$. **Right panel:** $t_f = 100000$, $N_{\text{ic}} = 25000$ and $M = 50$. Here, the numerical fitting gives $q \approx 3.539$ with $\chi^2 \approx 0.00057$.

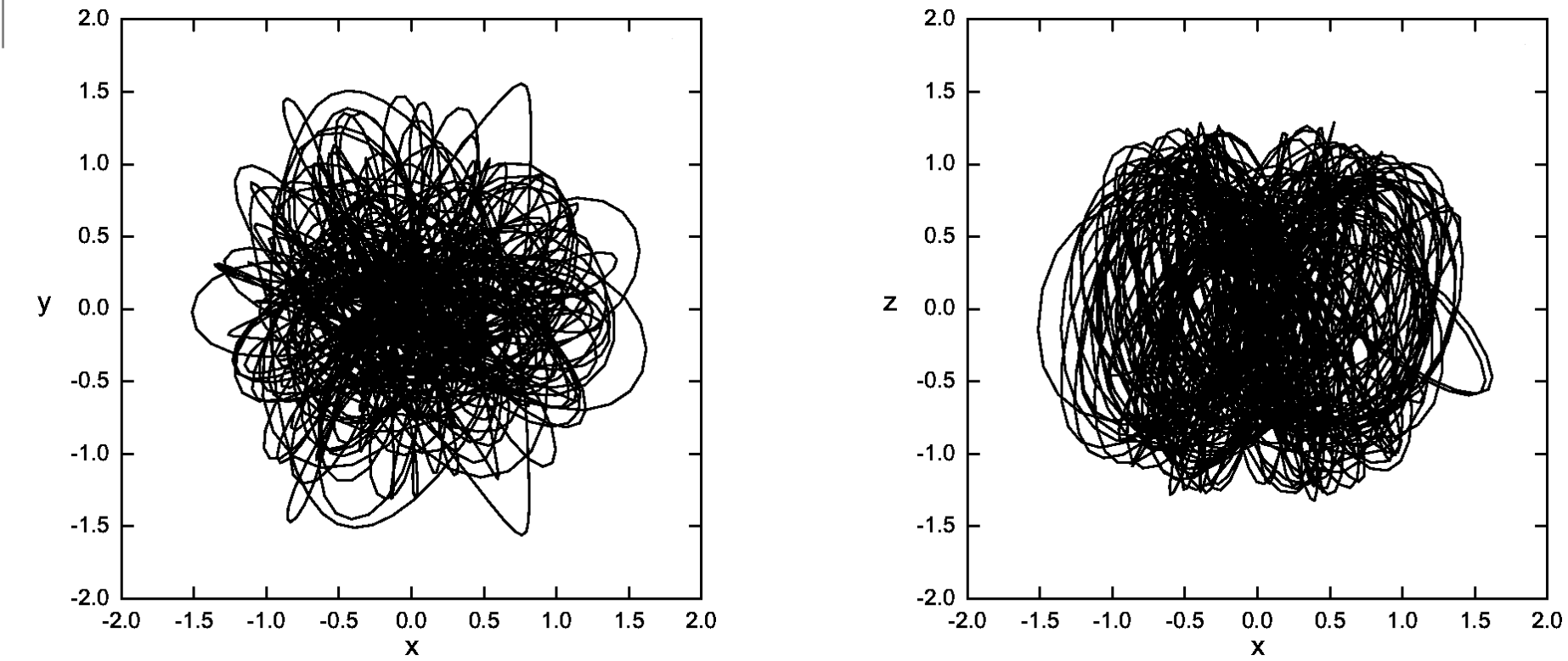

Figure 29: Left panel: Projections for the Chaotic Orbit 1 of the **3DOF Hamiltonian system** for **final integration time** $t_f = 10000$ in x, y and x, z **(right panel)**. Initial conditions: $(x, y, z, p_x, p_y, p_z) = (0.5875, 0, 1.291670, 0, 0, 0)$. $H = E = -0.285265450108748 1$.

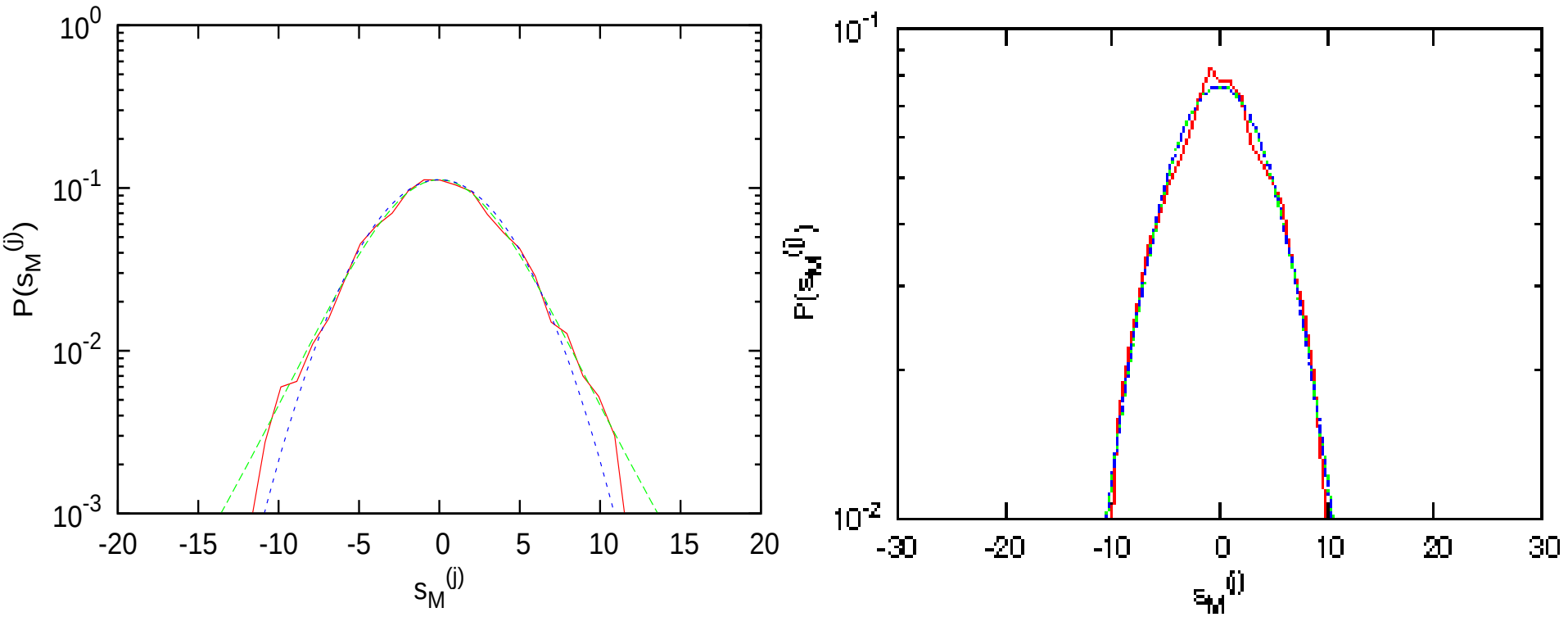

Figure 30: Pdf plots for the **Chaotic Orbit 1** of the 3DOF Hamiltonian system in linear-log scale of numerical (red curve), q-Gaussian (green curve) and Gaussian (blue curve) distributions. **Left panel:** $\eta = z$ **and** $t_f = 10000$ using $N_{\text{ic}} = 4000$ and $M = 50$ terms. Here, the numerical fitting gives $q \approx 1.25$ with $\chi^2 \approx 0.00017$. **Right panel:** $\eta = x + y$**,** $t_f = 100000$, $N_{\text{ic}} = 10000$ and $M = 100$ and fitting gives $q \approx 0.95$ with $\chi^2 \approx 0.00029$.

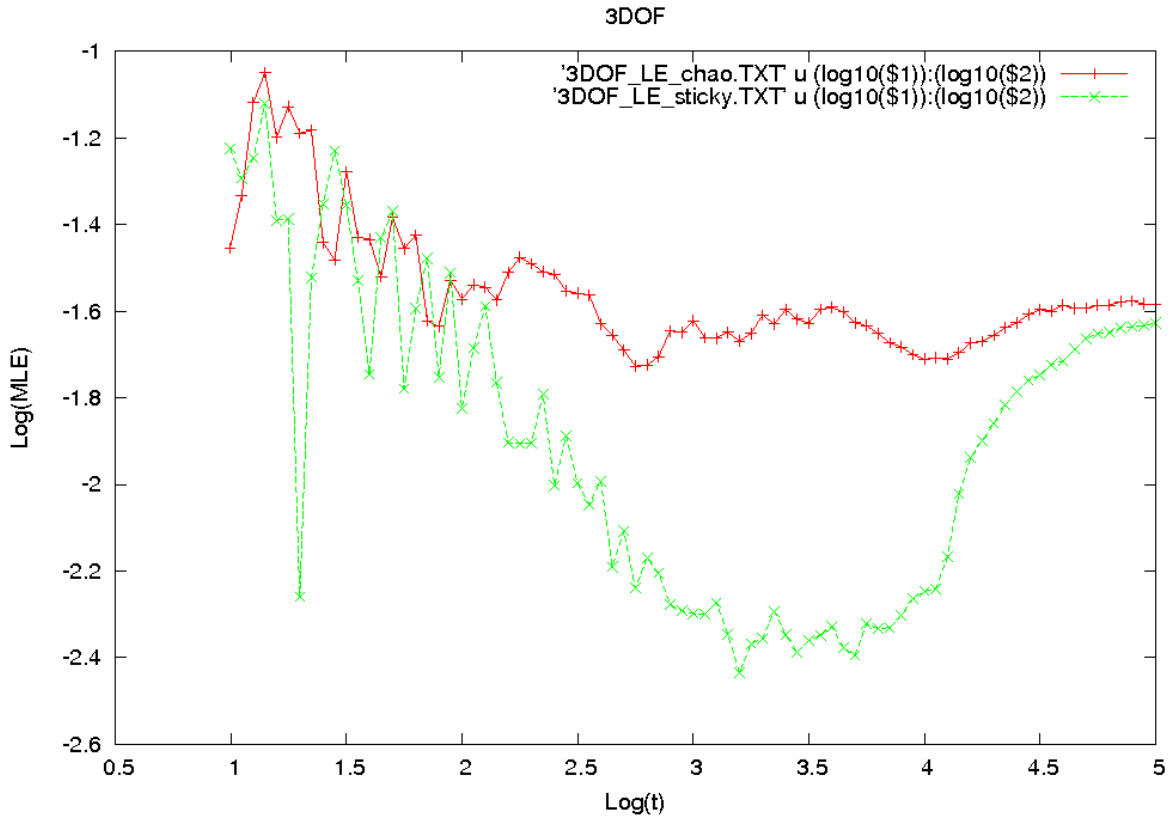

Figure 31: Maximum Lyapunov exponent evolution up to $t_f = 100000$ for the **Weakly Chaotic Orbit 2** of the **3DOF Hamiltonian system** (green curve) and **the Chaotic Orbit 1** of the same system (red curve).

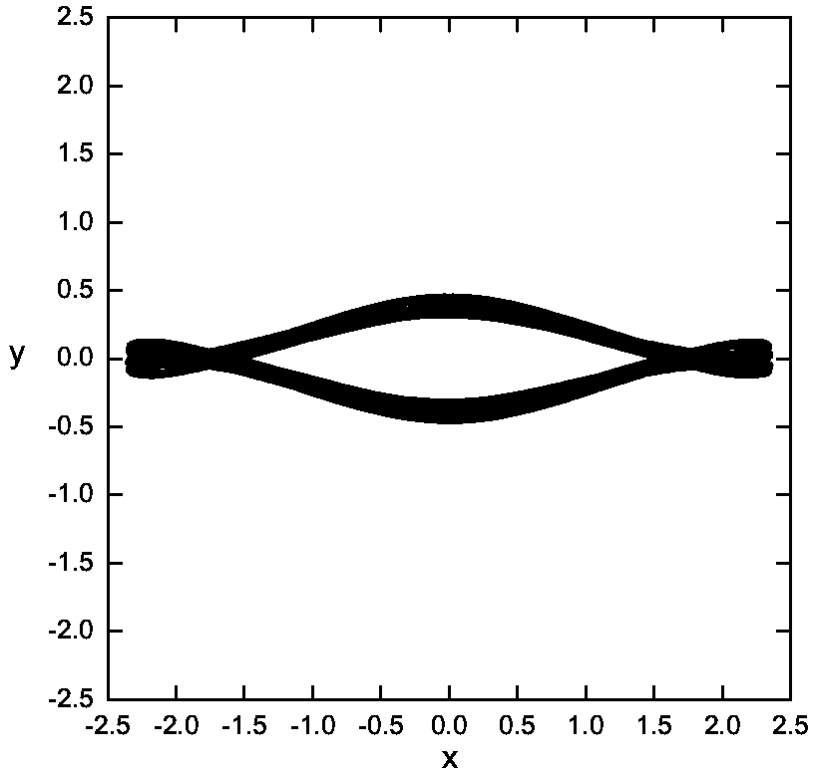

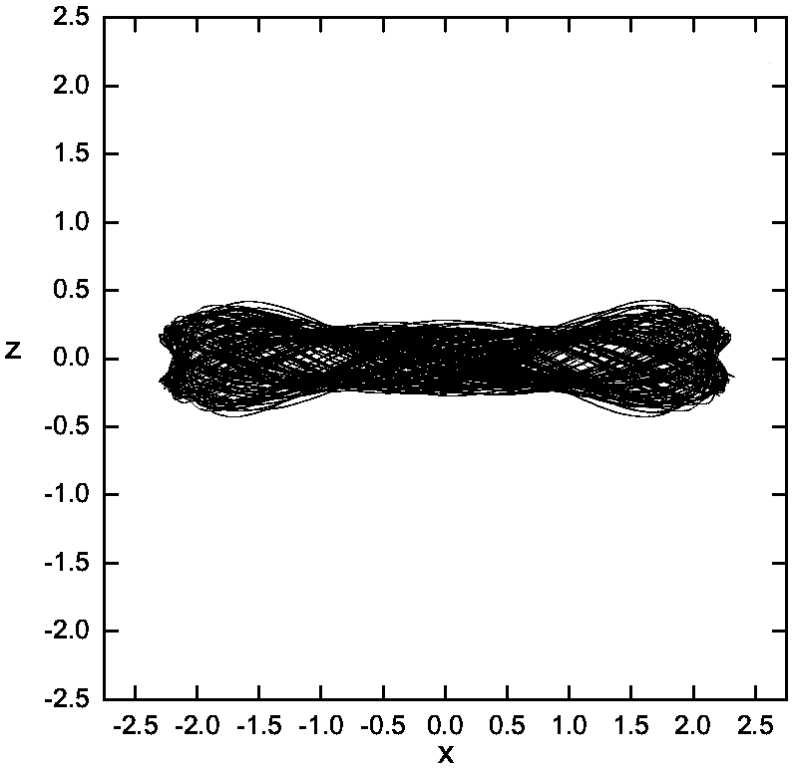

Figure 32: Projections for the Weakly Chaotic Orbit 2 of the **3DOF Hamiltonian system** for **final integration time** $t_f = 10000$ in x, y (left panel) and x, z (right panel). Initial conditions: $H = E = -0.2792149022676664$, $(x, y, z, p_x, p_y, p_z) = (2.35, 0, 0.08883, 0, 0.133330, 0)$.

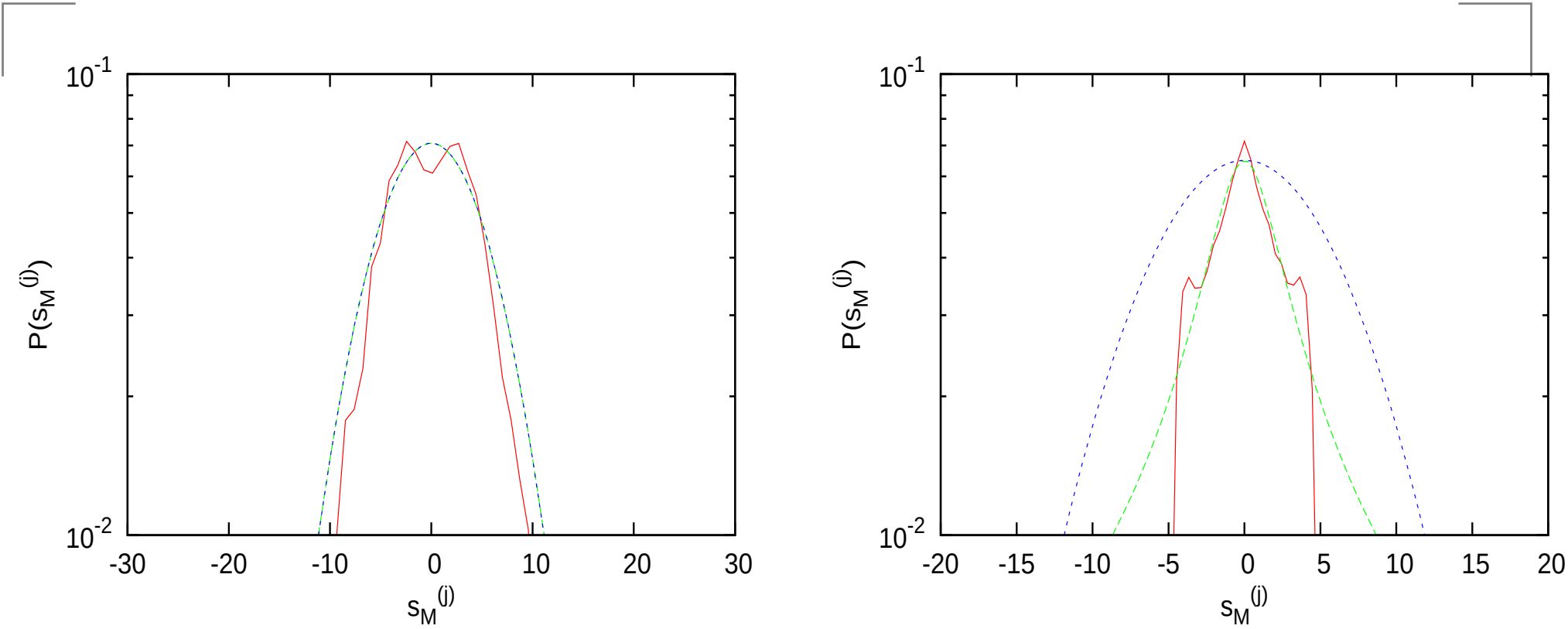

Figure 33: Pdf plots for the **Weakly Chaotic Orbit 2** of the **3DOF Hamiltonian system** in linear-log scale of numerical (red curve), q-Gaussian (green curve) and Gaussian (blue curve) distributions. **Left panel:** $\eta = z$ **and** $t_f = 10000$, with $N_{\text{ic}} = 4000$, $M = 50$ terms. **Right panel:** $\eta = x + y$**,** $t_f = 100000$, $N_{\text{ic}} = 10000$ and $M = 100$. In this case the numerical fitting with a q-Gaussian gives $q \approx 2.464$ with $\chi^2 \approx 0.00101$.

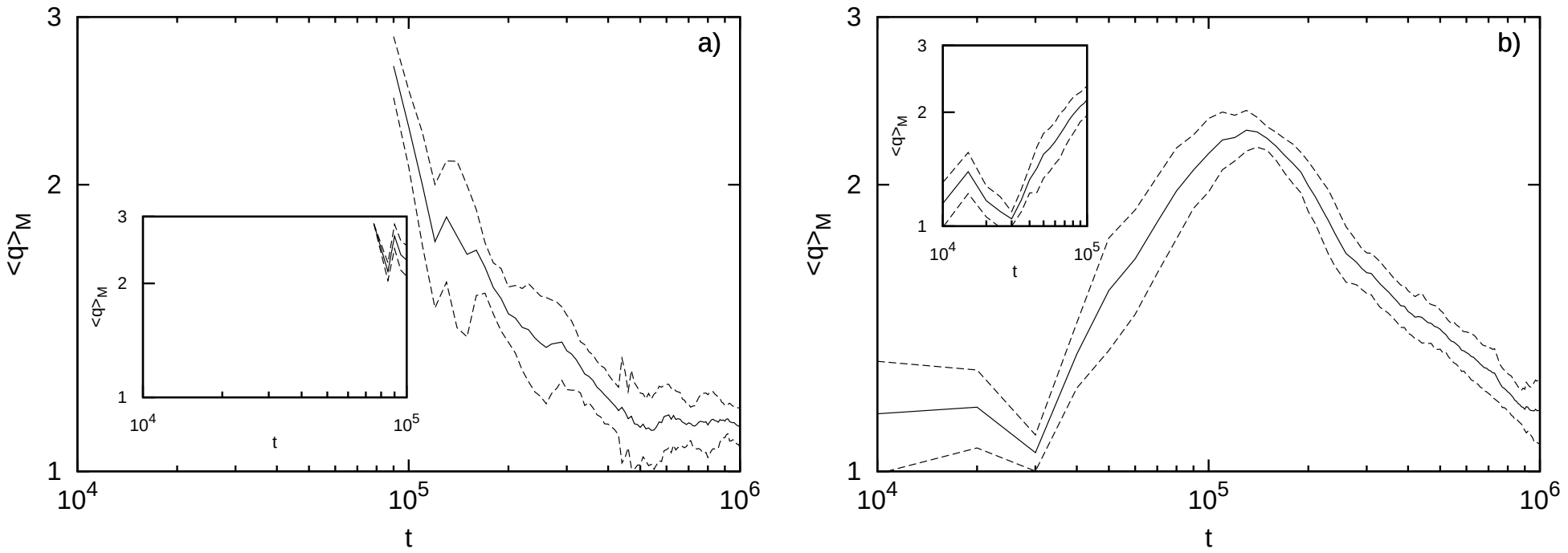

Figure 34: The time evolution of the $\langle q \rangle_M$-entropic parameter of the **Weakly Chaotic Orbit 2** of the 3DOF system (32) for $\eta = x + y$, $N_{ic} = 20000$ and $M = 50, 100, \ldots, 450, 500$. The dashed lines corresponds to one standard deviation from the average entropic parameter. The inset is a zoom-in up to $t_f = 10^5$. Panel b): Same as in panel a) but for $\eta = z$. These results have been verified by Fourier spectra calculations.

Conclusions

1. At **"weakly chaotic regimes"** located at the boundaries of islands of quasiperiodic motion of **Hamiltonian systems**, probability density functions (pdfs) of sums of chaotic variables, are **well approximated by q–Gaussians**.

2. These q–Gaussians are in fact **Quasi–Stationary States** (QSS) which **last for long times** and often pass through **different stages** to **exponential and finally to Gaussian form**.

3. In some cases, however, it is possible to find that the orbits **converge to a specific QSS**, whose pdf is **close to a q–Gaussian**, at least over its central part.

4. QSS approximated by q–Gaussians can be used to **identify weakly from strongly chaotic orbits** in **models of barred galaxies** over realistically **short time intervals**, where other methods, like Fourier analysis and Lyapunov exponents are not very helpful.

5. These results are also observed in **low–dimensional conservative maps** and multi-dimensional Hamiltonian systems **independent of the number of degrees of freedom**.

References

1. Tsallis, C. [2009], “Introduction to Nonextensive Statistical Mechanics: Approaching a Complex World”, *Springer, New York*.

2. Antonopoulos, C., **Bountis, T.** and Basios, V. [2011], “Quasi–Stationary States in Multidimensional Hamiltonian Systems”, Physica A, Vol. 390, 3290-3307. (2011).

3. Ruiz Lopez G., **Bountis, T.** and Tsallis, C. [2011], “Time–Evolving Statistics of Chaotic Orbits in Conservative Maps in the Spirit of the Central Limit Theorem”, Intern. J. Bifurc. Chaos, to appear (2012).

4. Tsallis, C. and Tirnakli, U. [2010], “Nonadditive Entropy and Nonextensive Statistical Mechanics – Some Central Concepts and Recent Applications”, *J. of Phys.: Conf. Ser.*, **201**, 012001.

5. Tassos Bountis, Chris Antonopoulos and Thanos Manos, “ Complex Statistics in Hamiltonian Models of Barred Galaxies”, to appear in Celestial Mechanics and Dynamical Astronomy (2012). http://arxiv.org/abs/1108.5059(2011).

6. Leo, M. and Leo, R. A. and Tempesta, P. [2010], “Thermostatistics in the Neighborhood of the π–mode Solution for the Fermi–Pasta–Ulam β System: From Weak to Strong Chaos”, *J. of Stat. Mech.: Th. & Exp.*, **04**, pp. 04021.

7. Antonopoulos, Ch., **Bountis, T.** and Skokos, Ch., [2006],“Chaotic Dynamics of N–Degree–of–Freedom Hamiltonian Systems”, *International Journal of Bifurcation and Chaos*, vol.**16**(6), 1777-1793 , June 2006.

8. Antonopoulos, Ch. and **Bountis, T.**, [2006], “Stability of Simple Periodic Orbits and Chaos in an FPU Lattice”, PRE**73**, 056206, 1-8 (2006).